Soil & Tillage Research 244 (2024) 106207

Contents lists available at ScienceDirect

Soil & Tillage Research

journal homepage: www.elsevier.com/locate/still

Measuring and modelling of soil displacement from a horizontal penetrometer and a sweep using an IMU sensor fusion and DEM

László Pásthy, Bence Szabó, Kornél Tamás *

Department of Machine and Product Design, Faculty of Mechanical Engineering, Budapest University of Technology and Economics, Műegyetem rkp. 3, Budapest H-1111, Hungary

ARTICLE INFO

Keywords:
Discrete element method
Parameter calibration
Horizontal penetrometer
Vertical penetrometer
Soil displacement sensor
Sweep

ABSTRACT

When simulating soil tillage processes using the discrete element method (DEM), it is essential to know the discrete element micromechanical parameters that describe the soil model, and this requires calibration. The formulation of a model that accurately reflects the behaviour of the soil from several perspectives is only possible by employing several different measurement procedures and DEM simulations. For this reason, four different measurements were used in this study for the purpose of calibrating the DEM model's micromechanical parameters for sandy soil with a dry based moisture content of 4.1 %. The cone penetration resistance was measured with a horizontal penetrometer that was developed in-house and a vertical penetrometer, while a displacement sensor placed in the soil provided information on the internal movement of the soil, and the draught force of a sweep tool was also monitored. The DEM models of the measurements were defined in Altair EDEM® software using the hysteretic spring contact model. To model the soil, spherical elements and clump elements were examined. The displacement sensor was modelled with a clump element, whereas the sweep tool and the horizontal and vertical penetrometers were taken into account as rigid surface models. Based on the simulations, it was determined that the clump elements examined are not suitable for proper calibration with the hysteretic-spring contact model, because, as a consequence of the large coordination number, they excessively increased the draught force by getting stuck in front of the tools and measuring devices. By studying sweep tool simulations, it was observed that, in terms of the particle sizes used, particles with a higher density and higher bulk density resulted in a higher draught force, but at the same time, they moved at a lower speed. Finally, by taking vertical penetrometer measurements and running simulations, the soil model created with spherical elements was validated with a relative error of 8.7 % which can describe the sandy soil with sufficient accuracy in all the examined aspects.

1. Introduction

As the frequency of periods of dry weather increases globally, the importance of conservation tillage methods is increasingly appreciated (Acharya et al., 1998; Bekele et al., 2022). Soil that is too compact has a low moisture retention capacity, and plants cannot develop properly in it. Therefore, being constantly aware of the level of soil compactness and keeping it at an appropriate value is of particular importance (Chen et al., 2005).

One way of gaining information about the compactness of the soil at a given moisture content and soil texture is to measure its cone penetration resistance (CPR) (Kim et al., 2008; Pires-Sturm and DeJong, 2023). There are two different variants of this measurement: The more widespread, standardised version is the vertical penetrometer measurement, during which the penetrometer cone is pushed vertically down (Kotrocz et al., 2016; Tamás and Bernon, 2021), and the other version is the horizontal penetrometer (HP) measurement in which a cone is moved horizontally through the soil (Alihamsyah et al., 1990). The vertical penetrometer measurement is suitable for characterizing soil compaction at specific points of the investigated area depending on the penetration depth (Kotrocz et al., 2016; Tamás and Bernon, 2021; Ucgul et al., 2014). Additionally, the vertical penetrometer measurements can be automatised to reduce the risk of human errors or inaccuracies. For example, Nisha et al. (2023) developed a hydraulic assisted embedded microprocessor-based cone penetrometer which can be mounted on the front of tractors and can be controlled with an android

* Corresponding author.
E-mail address: tamas.kornel@gt3.bme.hu (K. Tamás).

https://doi.org/10.1016/j.still.2024.106207
Received 22 March 2024; Received in revised form 27 May 2024; Accepted 8 June 2024
Available online 20 June 2024

mobile application.

However, with a vertical penetrometer, it is only possible to take samples at specific points in the investigated areas, which can often be a disadvantage. HP offers a solution to this problem, as it can measure CPR data at a certain depth, but along a continuous line. Hemmat et al. (2009) performed measurements with both a horizontal and a vertical penetrometer and found that if the results of both measurements show the same mode of soil failure (compressive), the correlation between the CPR values measured in the two directions is significant, although this is not feasible in all cases. Hall and Raper (2005) optimised the design of the HP tips they applied, taking into account the vertical oscillation of the tips, so that the measurements could be easily compared with vertical penetrometer measurements. Topakci et al. (2010) determined that HP measurements, in contrast to those obtained from a vertical penetrometer, offer more soil compaction data from the terrain, which provides a better opportunity to link the data to GPS coordinates and to create soil resistance maps of the investigated terrain. Naderi-Boldaji et al. (2013) developed a four-parameter statistical model for the estimation of dry bulk density, in which the CPR measured by HP and the moisture and clay content of the soil were taken into account.

Another possible approach to determining the compactness of the soil and ensuring its appropriate value is to utilise numerical simulations. One way to do this is to simulate HP measurements by applying the finite element method (FEM). Mouazen et al. (2003) developed an instrumented chisel that moved horizontally in the soil as a soil strength measurement device and conducted measurements and FEM simulations with it to estimate the peak force acting on the chisel and the dry bulk density. Naderi-Boldaji et al. (2013) developed a three-dimensional FEM model to model the interaction between a single-tip HP and the soil, which was used to investigate the effect of different measurement and simulation parameters on the CPR. Later, confirming the findings of Hemmat et al. (2009), Naderi-Boldaji et al. (2014) came to the conclusion, with the help of a FEM model creating simulations to investigate the soil failure mode, that the horizontal CPR depends on the depth of the tip and the distance of the tip from the tine. They also found that the FEM simulation allows for the measurement of CPR only when the penetration distance of the cone is relatively short.

In addition to FEM, measurement of the soil with a HP can also be simulated using the discrete element method (DEM), which enables the modelling of larger tool displacements (Ucgul et al., 2018; Zeng et al., 2020; Tamás and Bernon, 2021). The DEM is therefore widely used to run tillage simulations. Using a DEM model, Tamás and Bernon (2021) investigated the simulation of vertical penetration and the possibility of modelling the roots and the role of the root system in soil strengthening, a factor which can also be observed in soil-tool interaction. To date, however, based on our review of the literature, there have been no examples of HP measurement modelling with DEM.

Before running DEM simulations it is necessary to determine the DEM parameters of the soil, during which the non-measurable micromechanical parameters of the DEM model have to be set so that the bulk behaviour of the model closely matches the bulk behaviour of real soil (Tamás and Bernon, 2021). For example, when modelling a HP, the DEM parameters can be calibrated based on the CPR calculated as the ratio of the force acting on the penetrometer cone and the projected cross-section of the cone. However, a parameter set based on only one type of measurement does not necessarily model all characteristics of the soil with sufficient accuracy (Roessler et al., 2019). Therefore, to accurately calibrate the parameters, it is also necessary to take into account the results of several types of measurements (Tamás and Bernon, 2021). For example, while the draught force acting on a tool pulled through soil can be approximated with high accuracy in numerical simulations (Tamás et al., 2013; Ucgul et al., 2017), few studies have quantified how closely the movement of the simulated soil model matches the movement of real soil during the tillage process (Gürsoy et al., 2017; Milkevych et al., 2018; Zeng et al., 2020), even though this would be useful to know during DEM parameter calibration. Combining the measurements of the draught force acting on the tool pulled in the soil, the horizontal CPR and the internal movements in the soil is, therefore, a promising approach for ensuring a more accurate calibration of a discrete element model of the soil.

There are several methods for examining soil movement. The essence of the profilograph measurement procedure is to measure the initial and post-cultivation heights of the soil surface profile in a cross-section perpendicular to the moving direction of the tillage tool and then to compare the results of the two measurements. Hemmat et al. (2009) used a profilograph to examine the cross-section of the furrow formed after a HP measurement had been taken and showed that the failure planes of the soil and the horizontal CPR are related to each other. The advantage of profilograph measurements is that they provide a quick and relatively cost-effective solution for characterizing the soil surface, but a disadvantage of these measurements is that they do not provide information about the internal movements of the soil.

In essence, using passive markers involves placing different, uniquely marked, small markers in the soil in the path of the tillage tool, in specific positions, then measuring their displacements after the tillage process (Gürsoy et al., 2017; Milkevych et al., 2018). The advantage of the procedure is that it is cost-effective and suitable for testing different soil layers, but it has the disadvantage that placing markers in the ground requires time-consuming and precise work. A further disadvantage of passive markers is that only the initial and final positions can be determined, thus this method does not provide information about the path travelled by the soil during the measurement.

A possible solution to this shortcoming could be to use tracers with active sensors which can measure their acceleration in real time, from which the trajectory of the tracer can be determined by double time integration (Wágner et al., 2023). Active tracers have already been used in the measurement of the movement of glass balls in a mixing drum (Marigo et al., 2013) and in a study of the mixing of liquid solutions (Bruno et al., 2024), although the positron emission particle tracking (PEPT) method used in these studies can only measure small displacements (0–100 mm), and its significant cost does not allow it to be used widely in industrial applications. Based on a thorough literature review, it appears that the first, and so far only, real time analysis of internal soil movements effected by the soil-sweep tool interaction was carried out by Wágner et al., (2023), who used an active tracer which was a magnetic angular rate gravity (MARG) sensor, developed in-house and presumably easily reproducible.

Based on the shortcomings found in the literature, our aims were to carry out measurements of the soil using an in-house developed HP measuring device, with a displacement sensor that can be placed in the soil, similar to that developed by Wágner et al. (2023), with a sweep tool and a vertical penetrometer. We would subsequently create a DEM model of the measurements and evaluate the accuracy of sweep tool resistance and soil movement simulations where DEM parameters were calibrated using horizontal penetrometer measurements and verified by vertical penetrometer measurements.

2. Materials and methods

2.1. Measurements

The empirical measurements were taken in a laboratory soil bin facility located at the Institute of Technology of the Hungarian University of Agriculture and Life Sciences in Gödöllő. The size of the soil bin was 50 m long, 1.95 m wide and 2 m deep. Sandy soil was used, as it is more homogenous than clay soil, and it is thus easier to ensure adequate moisture content and an even surface, as well as to place the soil displacement sensor in the desired position. The soil bin was filled with sandy soil (93.28 % sand, 4.66 % silt and 2.06 % clay) (Tamás et al., 2013) with a dry based moisture content of 4.1 %, and measurements were taken in the soil-filled bin.

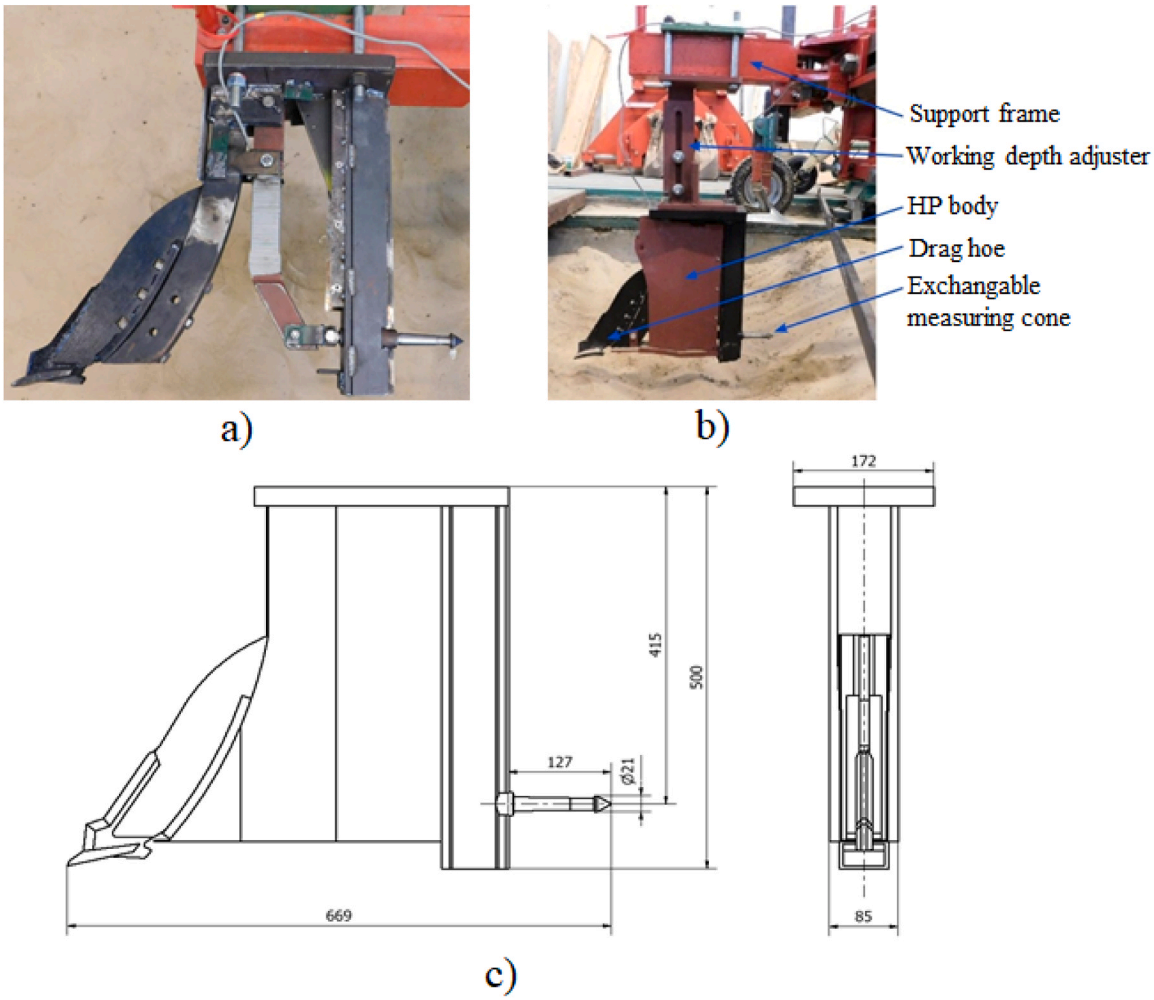

Fig. 1. Horizontal penetrometer a) internal structure, b) parts and c) inclusion dimensions of measuring device (dimensions are in mm).

2.2. *Horizontal penetrometer*

The HP developed for this research is shown in Fig. 1, the main parts of which are the body (tine), the measuring cone, the depth adjuster, and the draw-in hoe. The entire measuring device can be attached to a measuring frame. The mechanism and measuring device that measures the force acting on the measuring cone is housed inside the body. The design allows the use of measuring cones with different geometries and sizes. During field measurements, the draw-in hoe helps to push the penetrometer body into the soil backwards, as the edges of the hoe open the soil by cutting it, thus making it easier for the penetrometer body to enter the soil. To determine the horizontal CPR, a shank equipped with strain gauges was used (Tamás, 2018). The support rod of the measuring cone was connected to this shank by a two-hinged connecting element, which allowed harmful stresses to be avoided.

During the measurement of the horizontal CPR, the HP was moved horizontally in the soil at a depth of 0.25 m and at a pre-determined average speed of 0.5 ms^{-1} with a standard deviation of 0.043 ms^{-1}. Meanwhile, the force acting on the measuring cone with a projected cross section of 3.33 cm^2, a cone base diameter of 2.06 cm and a cone angle of 60° was measured at a frequency of 100 Hz.

2.3. *Displacement measuring sensor*

The investigation of the soil movement was carried out based on the principle of acceleration measurement. A microelectromechanical inertial measurement unit (IMU) sensor was used to measure acceleration (Wágner et al., 2023). In addition to an accelerometer, such devices also contain a gyroscope and may contain a magnetometer, in which case they can also be referred to as a magnetic angular rate gravity (MARG) sensor. The sensor used in our research was a MARG sensor, as it is suitable for determining not only acceleration, but also spatial orientation. Another advantage of MARG sensors is that they are readily available on the market.

The displacement measurement and evaluation system developed for this study can be divided into three parts (Wágner et al., 2023). The first part is the displacement sensor (Fig. 2. a, b and d), which is placed in the soil during the measurements, and which collects data in real time. The second is the software used to control the measurements (Fig. 2. c), while the third element is the software used for data processing (Fig. 2. c).

Inside the displacement sensor is an IMU sensor, a microcontroller unit (MCU) with WiFi connectivity, and a battery required for power supply (Fig. 3. a). These components are located in a 3D printed housing, as shown in Fig. 2. b.

The task of the MCU is to receive and execute commands from the measurement controller, as well as to transmit the data collected. With the utilisation of WiFi, there is no need for a wired connection between the data collector and the computer running the measurement control software and processing the data.

During the measurement and data processing, the path of the data is shown in Fig. 2. c). It is observable that within the IMU sensor there are three sub-sensors, including a magnetometer (±2.5° accuracy, 0,3 μT resolution, 1 %FS full scale nonlinearity), a gyroscope ($125°s^{-1}$ rate

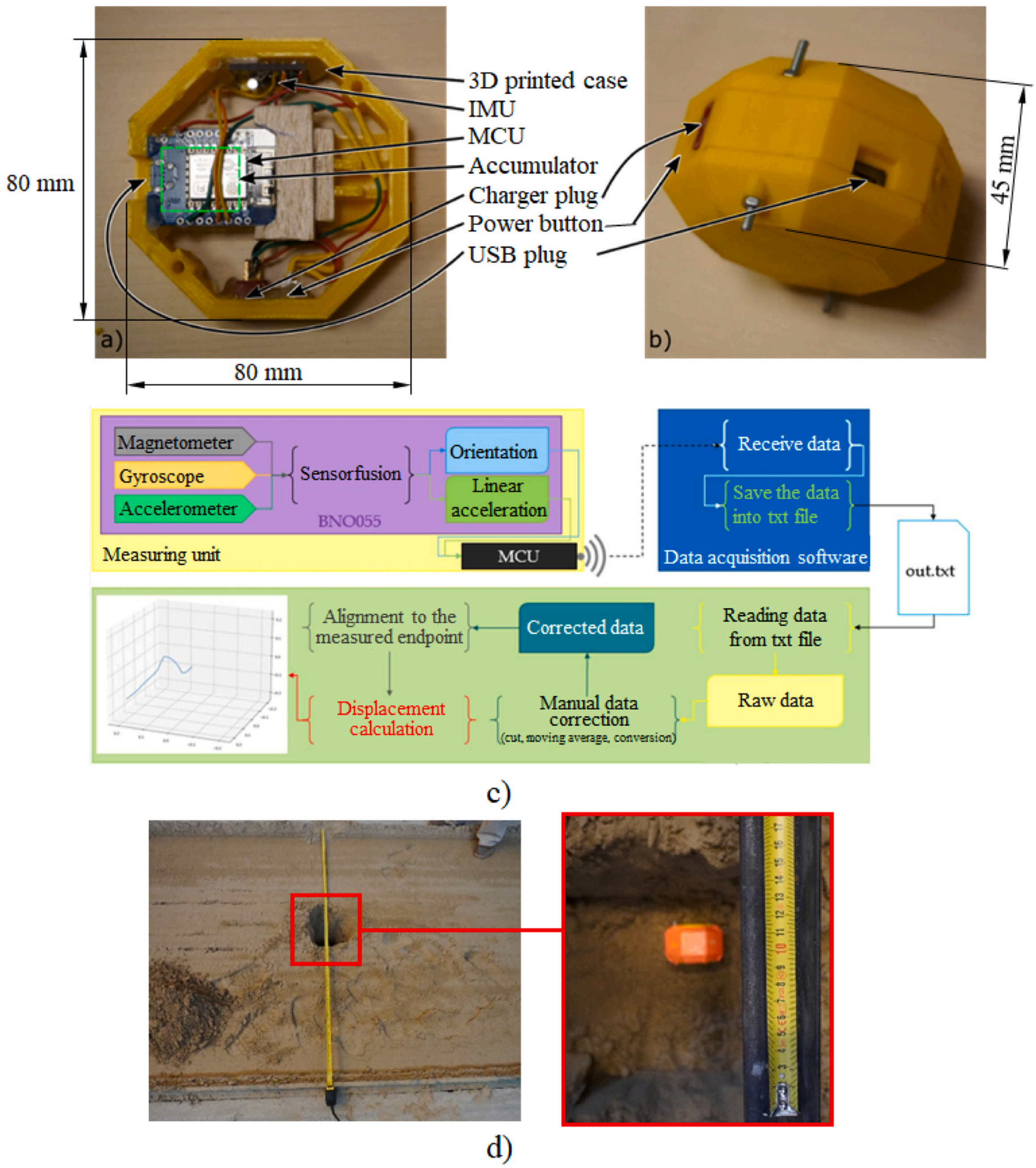

Fig. 2. Displacement sensor, a) internal and b) external structure, c) flowchart of data extraction and processing, d) placement in the soil.

range, 900 rads^{-1} sensitivity) and an accelerometer (±19.62 ms^{-2} measurement range, 1 LSB mg^{-1} sensitivity) (Wágner et al., 2023). Furthermore, there is also a built-in microcontroller unit (MCU) which performs a sensor fusion and combines the received data from the three sensors. The data is next sent to a data acquisition software application via the WiFi connection, where it is saved. Later the raw acceleration data is filtered, integrated twice in the function of time and with the manual specification of the start and endpoints of the device in the measurement the trajectory path can be obtained.

One of the three sensors, the magnetometer, was turned off, because the steel HP body would have interfered with the magnetic field. The displacement measuring sensor was then placed in the soil at a depth of 200 mm in the middle of the measuring section in the vertical symmetry plane of the measuring cone of the HP (Fig. 2. d). The displacement data were recorded at a frequency of 150 Hz, independently from the horizontal CPR data and the velocity data of the measuring cart.

2.4. Sweep tool

To carry out the HP measurement, a sweep tool was also pulled through the soil bin parallel to the HP (Fig. 3.). The sweep tool was placed in the soil at the same depth of 0.25 m as the cone of the HP. During the measurement, the force acting on the tool was measured using strain gauges, similarly to the measurements of Tamás (2018).

2.5. Vertical penetrometer

In addition to the HP measurements, measurements were also taken with a vertical penetrometer (06.15.SA, Royal Eijkelkamp B.V., Netherlands, 0–1000 N measuring range, 1 N force resolution), at 5 randomly chosen points of the soil bin, using a measuring cone with a projected cross-section of 1 cm^2, a base diameter of 1.13 cm^2, and a cone angle of 60°. The measurement speed of the penetrometer was lower

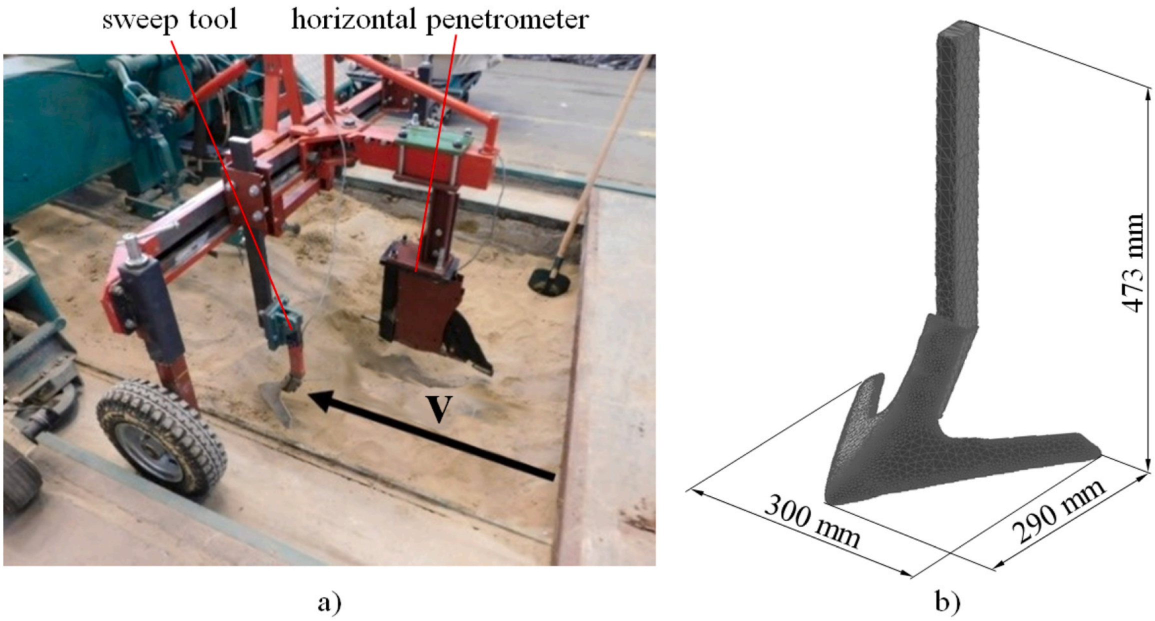

Fig. 3. Soil sweep tool measurement, a) initial state of the sweep tool and the HP (the direction of the measurement is indicated by the velocity vector **v**, b) inclusion dimensions of the sweep tool.

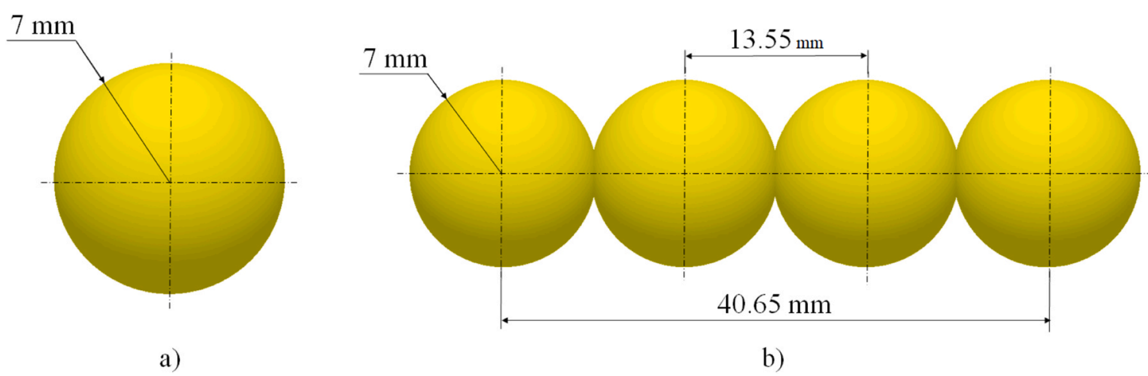

Fig. 4. Particles used for soil modelling, a) spherical particle, b) clump particle built up from 4 spheres.

than 20 mms^{-1} in accordance with the ASABE standards (ASABE Standards, 2006a, 2006b).

2.6. DEM simulations

The measurements were simulated using the DEM using Altair EDEM 2020® software. The soil was modelled by applying a combination of hysteretic spring and linear cohesion contact models (Bahrami et al., 2020; Ucgul et al., 2015). To model the soil, two types of elements were used: Firstly, spherical particles with an average radius of 7 mm and standard deviation of 0.035 mm (Fig. 4. a) were examined. Secondly, as several previous studies have concluded that the inhomogeneity of the soil and the irregular shape of soil particles can be better taken into account by including clump elements (Grabowski et al., 2021; Katagiri, 2019; Yang and Huang, 2023), clump elements were also examined. In a study conducted by Tamás and Bernon (2021) using elongated clump elements composed of 4 spheres proved to be an effective approach to modelling soil particles, so the same clump element shape with a 7 mm average radius and 0.035 mm standard deviation spheres (Fig. 4. b) were also utilised in this study. The displacement measuring sensor was modelled with a clump element built up from spheres (Fig. 5c). The walls of the soil bin, the HP, the sweep tool and the vertical penetrometer were modelled with rigid surfaces built up of triangular elements. The 3 m long, 0.7 m wide, 0.5 m deep particle assembly modelling the soil (Fig. 6a) was created by gravitational deposition. After that, the particles in the centre of the assembly were removed, to a depth of 0.2 m, in area 0.08 m long and 0.7 m wide, and the clump model of the displacement meter was placed at a depth of 0.2 m, symmetrically to the length and width of the assembly (Fig. 6b and c). Then, in order to be able to track the movement of the soil layer above the displacement sensor, the particles above the clump model of the displacement sensor were coloured yellow (Fig. 6c).

2.7. Simulation of HP and displacement sensor measurement

For the DEM simulations, the same geometry was used as for the empirical HP measurement. The model of the HP was placed in front of the DEM assembly so that the cone of the penetrometer was at a depth of 0.25 m, then during the simulation, it was moved through the particle assembly at a rate of 0.5 ms^{-1}. In order to investigate the effect of the penetrometer body on the horizontal CPR, simulations using spherical particles with 2000 kgm^{-3} solid density were also run with the penetrometer body removed and only the cone present. During the simulations, the force acting on the penetrometer cone was recorded, which was divided by the projected cross-section of the penetrometer to calculate the horizontal CPR. The trajectory of the displacement sensor

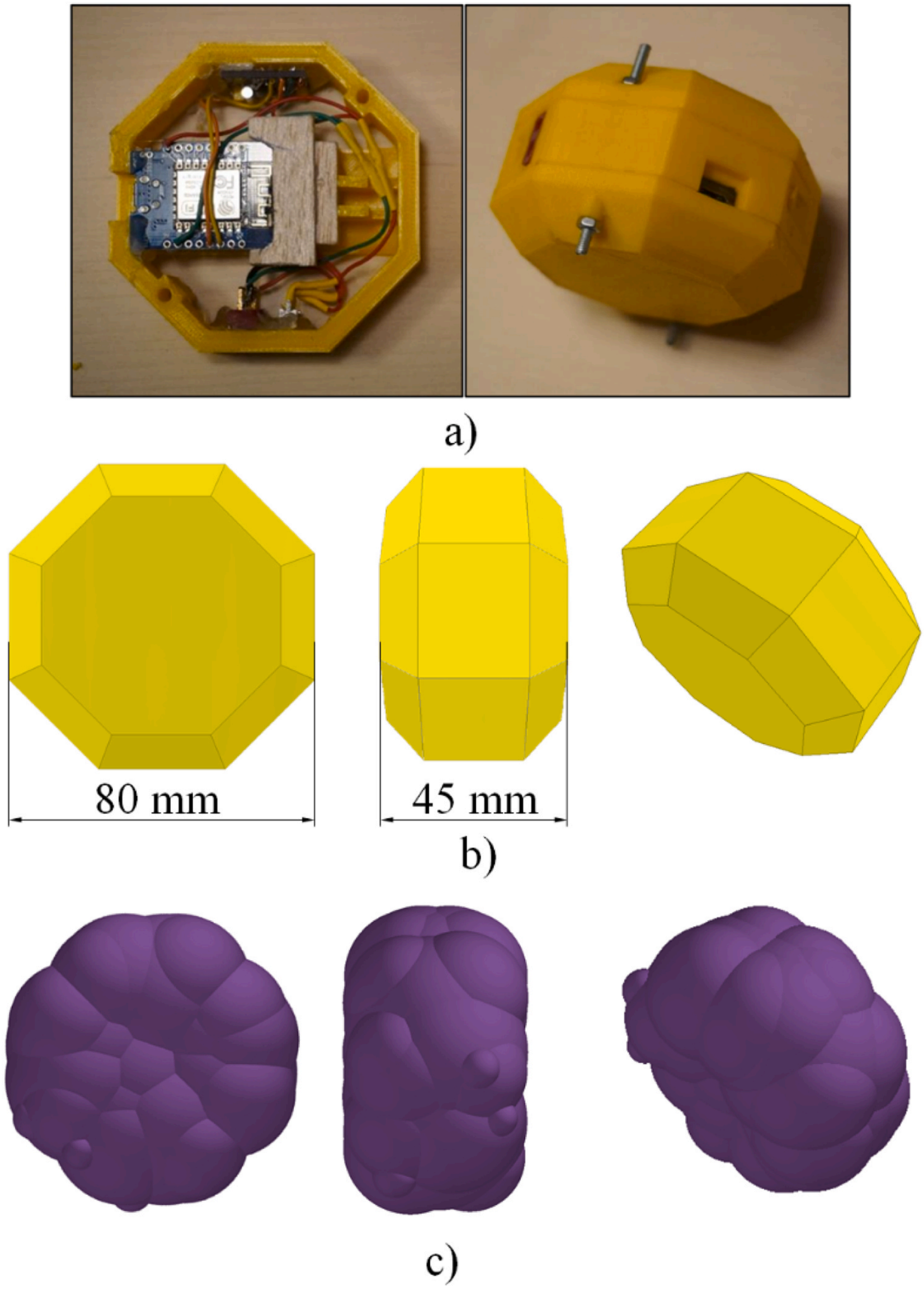

Fig. 5. Displacement sensor a) photo, b) CAD model, c) clump model built up from spheres.

was also recorded along the three spatial axes. In order to compare the measured and simulated trajectory path, the distance to the nearest point of the measured path was determined at each data point of the simulated path, and by averaging these distance values and dividing by the length of the measured path, the percentage deviation of the simulated path from the measured path was determined.

2.8. Simulation of the sweep tool measurement

The initial state of the DEM simulations of sweep interaction is shown in Fig. 7. As with the empirical measurements, the tool was placed at a depth of 0.25 m and was moved horizontally at a speed of 0.5 ms^{-1} over a length of 3 m. During the simulations, the force acting on the tool was recorded as a function of the tool's displacement. Furthermore, in the simulations, the model of the displacement sensor was also placed in the particle assembly in the same position as in the HP simulations, and its trajectory path was recorded. Since the displacement sensor was not placed in the soil during the measurement of the soil-sweep interaction, it was not possible to compare the simulated trajectory path with the measured data. However, it was possible to compare the trajectory paths resulting from the different simulations with each other.

2.9. Simulation of vertical penetrometer measurement

The DEM simulation of the vertical penetrometer measurements was performed with five penetrometer geometries placed 0.5 m apart from each other above the particle assembly (Pásthy et al., 2024). Similarly to the measurements, the penetrometer geometries were moved vertically downwards at a speed of 20 mms^{-1} (Fig. 8. a). The angle of the

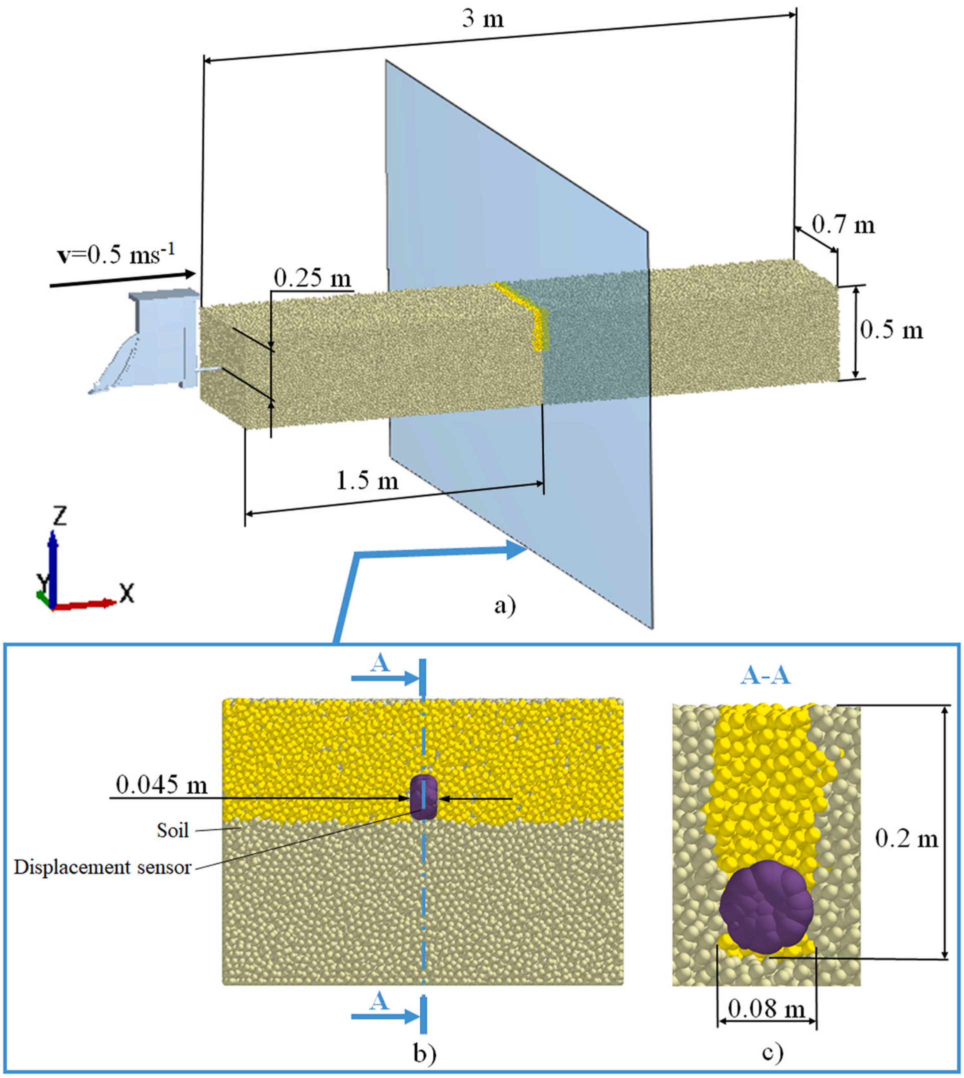

Fig. 6. Initial state of the HP and soil displacement sensor simulation in the case of the spherical particle assembly, a) dimensions of the DEM assembly and placement of the HP, position of the displacement sensor b) in the lateral mid-section c) in the longitudinal mid-section of the DEM assembly (the velocity of the HP is indicated by vector **v**).

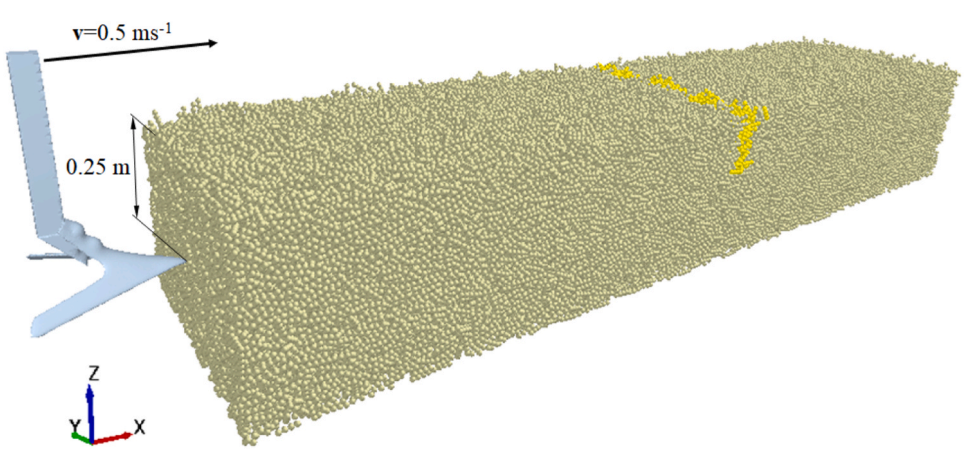

Fig. 7. Initial state of the soil sweep interaction in the case of the clump particle assembly (the velocity of the tool is indicated by vector **v**).

measuring cone was also 60°, the same as the measurements. However, in contrast to the projected cross-section of 1 cm^2 used in the measurements, the projected cross-section of the measuring cone was 38.5 cm^2 (Fig. 8. b). This change was made necessary by the particle size used in the simulations, because if the measuring cone had been comparable to the particle size, it could have resulted in a fluctuating CPR

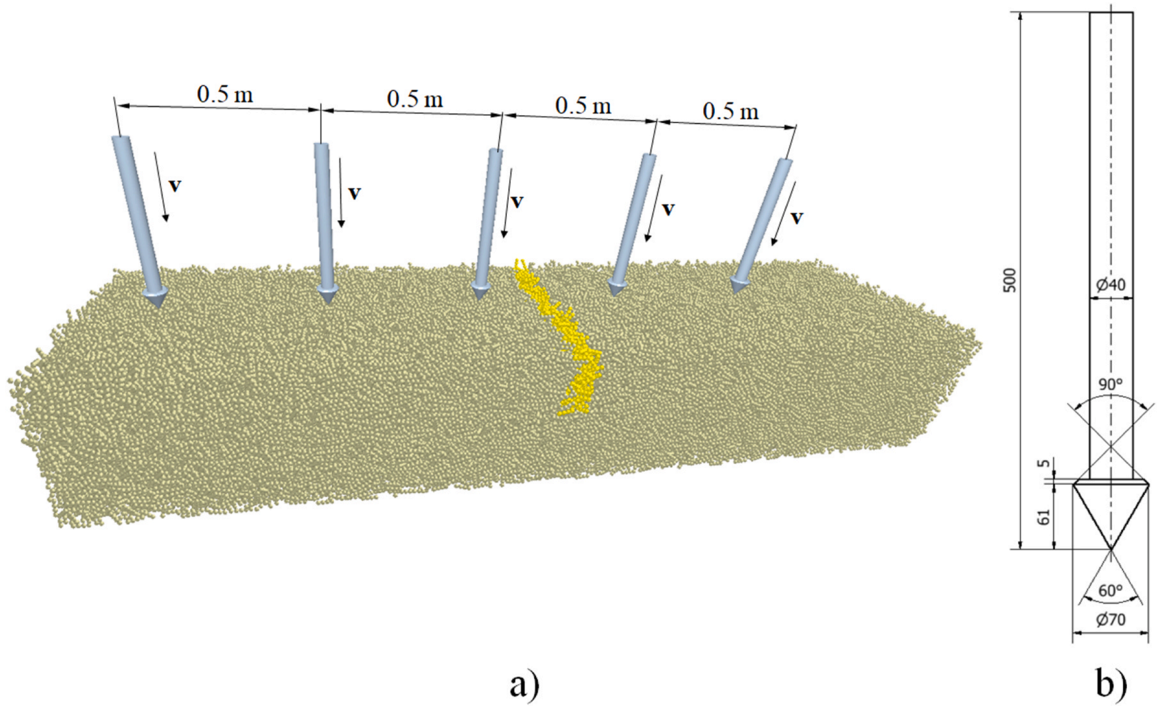

Fig. 8. Simulation of the vertical penetrometer measurement, a) initial state in the case of the clump assembly (the velocity of the penetrometer is indicated by vector **v**), b) geometry and sizes of the penetrometer used in the simulations (dimensions are in mm).

Table 1
Calibrated micromechanical DEM parameters.

Materials	Soil particles	Displacement sensor	Wall and tools
Particle radius [mm]	6.965–7.35 selected	-	-
Particle size distribution	random	constant	-
Solids density [kgm^{-3}]	2900 and 2000 calibrated	2500 selected	2500 selected
Mass [kg]	calculated	0.0856 measured	not relevant
Young's modulus [Pa]	$2.10 \bullet 10^9$ selected	$1.875 \bullet 10^8$ selected	$2.5 \bullet 10^8$ selected
Shear modulus [Pa]	$7.5 \bullet 10^8$ selected	$7.5 \bullet 10^7$ selected	10^8 selected
Poisson's ration [-]	0.4 selected	0.25 selected	0.25 selected
Yield strength [Pa]	10^7 selected	$5.35 \bullet 10^5$ (Ucgul et al., 2015)	-

Table 2
Micromechanical DEM parameter pairs in case of spherical particles.

Material pairs	Soil particles - Soil particles	Soil particles -Displacement sensor	Soil particles - Wall and tools	Displacement sensor - Wall and tools
Coefficient of restitution [dimensionless]	0.6 (Ucgul et al., 2015)	0.1 selected	0.6 (Ucgul et al., 2015)	0.1 selected
Static friction coefficient [dimensionless]	0.49 calibrated	0.5 (Ucgul et al., 2015)	0.7 (Yang et al., 2022)	0.5 (Ucgul et al., 2015)
Rolling friction coefficient [dimensionless]	0.39 calibrated	0.01 selected	0.6 (Yang et al., 2022)	0.01 selected
Damping factor [dimensionless]	0.5 (Pásthy et al., 2024)	0.5 (Pásthy et al., 2024)	0.5 (Pásthy et al., 2024)	0.5 (Pásthy et al., 2024)
Stiffness factor [dimensionless]	0.85 (Pásthy et al., 2024)	0.85 (Pásthy et al., 2024)	0.85 (Pásthy et al., 2024)	0.85 (Pásthy et al., 2024)
Energy density [Jm^{-3}]	400,000 selected	8000 (Yang et al., 2022)	400,000 selected	8000 (Yang et al., 2022)

profile (Kotrocz et al., 2016) as well as higher-than-real CPR values (Tamás and Bernon, 2021). It is also evident that when a sufficiently large projected cross-section is chosen, the CPR values are not affected by the projected cross-section (Tamás and Bernon, 2021), therefore the measured and simulated CPR values remained comparable despite the different cross-sections. In order to compare the measured and simulated results, the correlation coefficient between the measured and simulated CPR-depth curves was calculated using the built-in function of Microsoft

Table 3
Micromechanical DEM parameter pairs in case of clump particles.

Material pairs	Soil particles - Soil particles	Soil particles -Displacement sensor	Soil particles - Wall and tools	Displacement sensor - Wall and tools
Coefficient of restitution [dimensionless]	0.6 (Ucgul et al., 2015)	0.1 selected	0.6 (Ucgul et al., 2015)	0.1 selected
Static friction coefficient [dimensionless]	0.24 calibrated	0.5 (Ucgul et al., 2015)	0.7 (Yang et al., 2022)	0.5 (Ucgul et al., 2015)
Rolling friction coefficient [dimensionless]	0.2 calibrated	0.01 selected	0.6 (Yang et al., 2022)	0.01 selected
Damping factor [dimensionless]	0.5 (Pásthy et al., 2024)	0.5 (Pásthy et al., 2024)	0.5 (Pásthy et al., 2024)	0.5 (Pásthy et al., 2024)
Stiffness factor [-]	0.85 (Pásthy et al., 2024)	0.85 (Pásthy et al., 2024)	0.85 (Pásthy et al., 2024)	0.85 (Pásthy et al., 2024)
Energy density [Jm^{-3}]	400,000 selected	8000 (Yang et al., 2022)	400,000 selected	8000 (Yang et al., 2022)

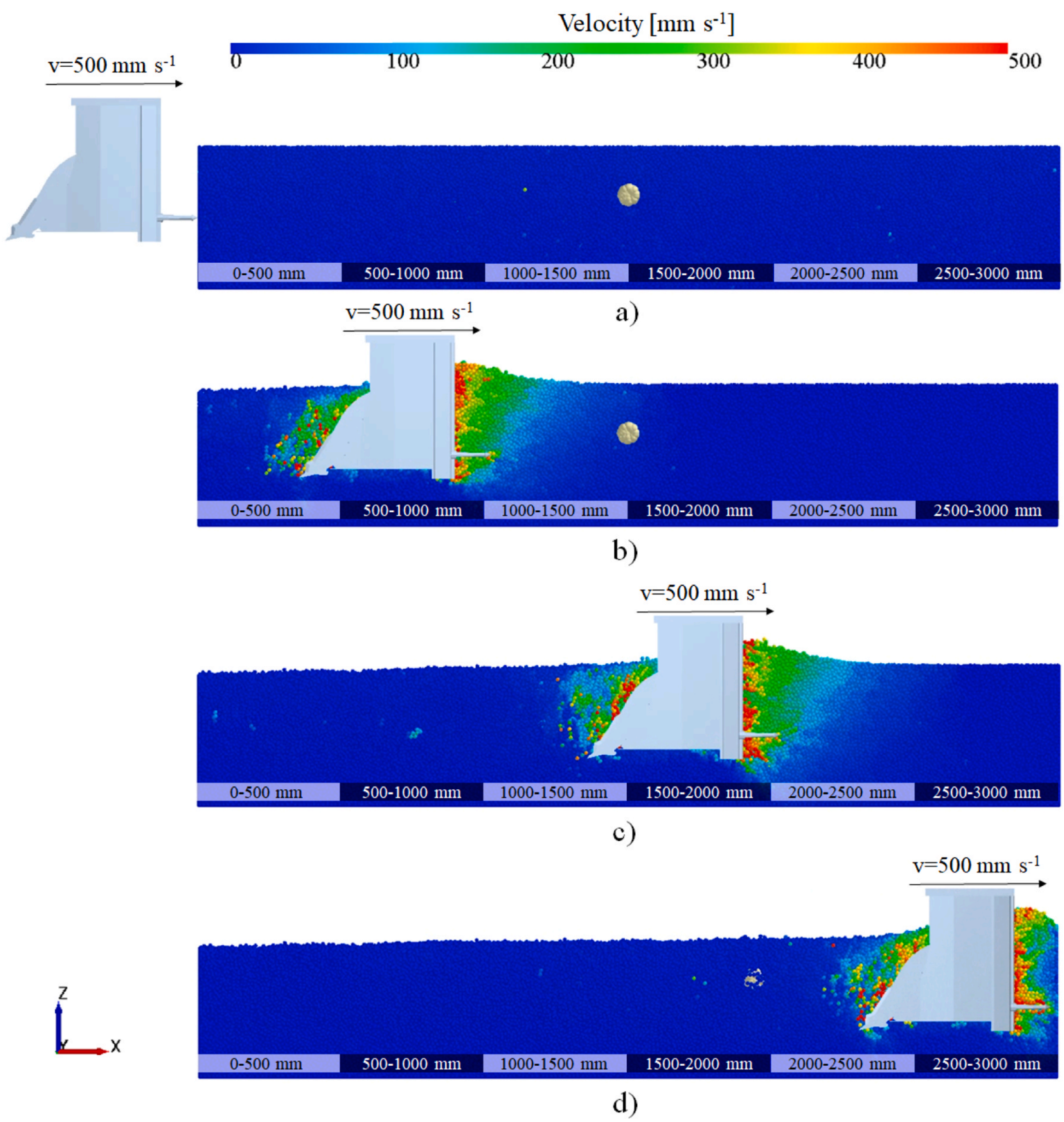

Fig. 9. Velocity of the assembly with spherical particle shape and 2900 kgm^{-3} density at a) 0 mm, b) 1000 mm, c) 2000 mm and d) 3000 mm HP displacement (the velocity of the HP is indicated by vector **v**).

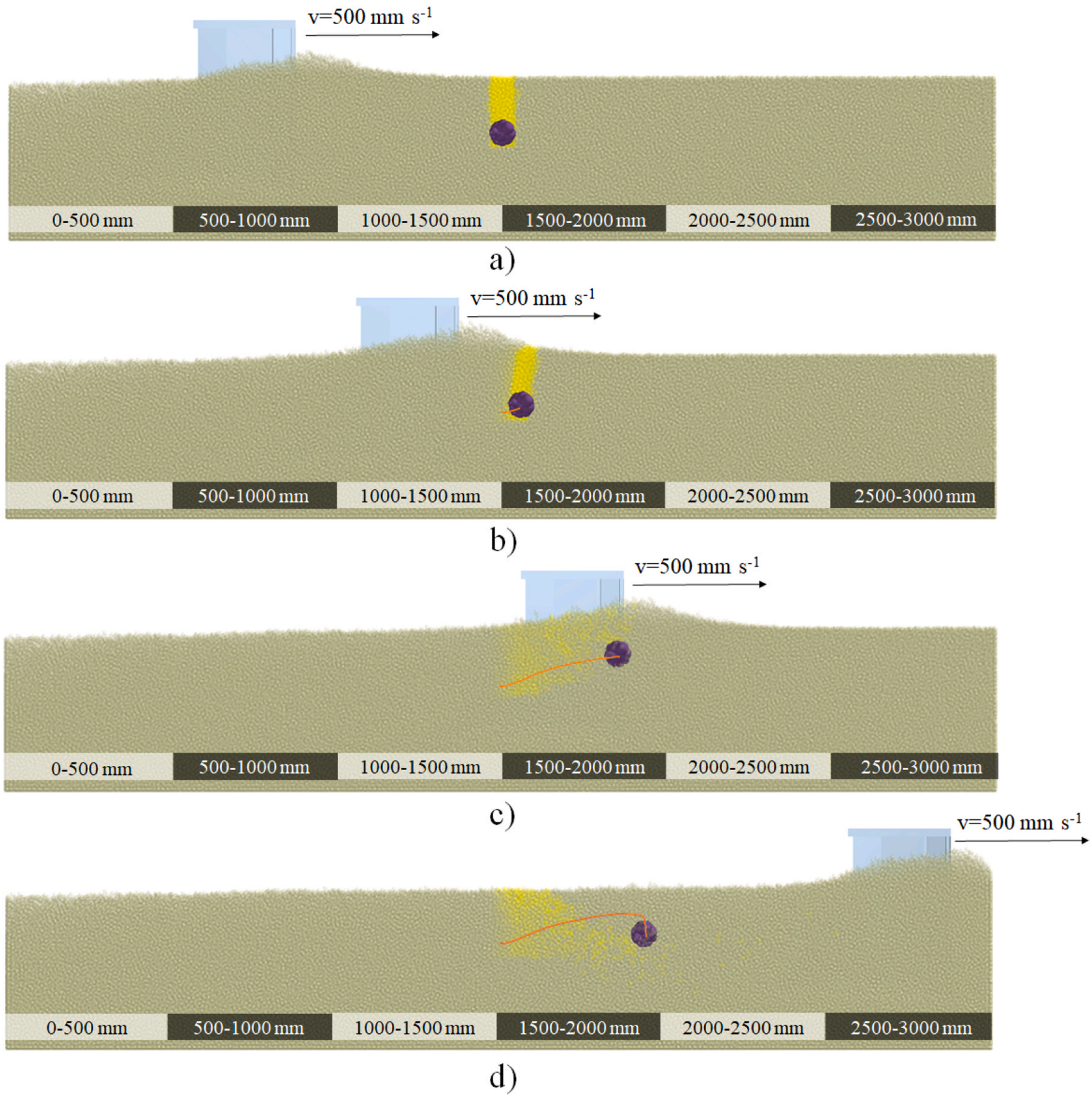

Fig. 10. Movement of the displacement sensor in the simulation of the HP measurement with spherical particle shape and 2900 kgm^{-3} density at a) 1000 mm, b) 1500 mm, c) 2000 mm, d) 3000 mm HP displacements (due to the visibility of the displacement sensor, the soil particles and the HP were made 90 % transparent, the velocity of the HP is indicated by vector **v**, the trajectory path of the displacement sensor is indicated by an orange line, and the particles which were initially above the displacement sensor are coloured yellow).

Excel® 2013, which was subtracted from 100 % and multiplied by −1 to give the correlation error.

2.10. Material parameters

As no standard calibration test results (such as from a direct shear box test or a confined compression test) were available, the cohesion and internal friction coefficient of the soil could not be directly obtained and used for calculating the friction and cohesion parameters of the DEM models. For this reason, a different calibration approach was utilised. In a study by Pásthy et al. (2024) the DEM parameters were calibrated effectively with the modification of static and rolling friction coefficients until an appropriate agreement was found between the simulations and measurements. A similar approach was therefore used to calibrate the DEM parameters in this study too, namely the friction parameters and the energy density of the material pairs were modified separately for both examined soil particle shapes (spheres and clumps) until good agreements were found in the simulations and measurements of the steady-state mean values of horizontal CPR. Nevertheless, the obtained parameter combinations do not rule out the possibility that a suitable match with the measured horizontal CPR value would also occur with another parameter combination. Therefore, in a subsequent study, it would be worth searching for several possible parameter combinations, for example with the help of stochastic search algorithms (Cheng et al., 2018; Do et al., 2017), from which the parameter combinations containing the highest proportion of the values expected for real soil could be selected. However, the simulations of the soil-sweep interactions run with the resulting parameter combinations did not show a good agreement with the measured draught force. This can be explained by the fact that the sweep tool was of much larger dimensions, so the tool size – particle size ratio was much higher than the HP cone size – particle size ratio, which resulted in different contact behaviour with the particle assembly, therefore the original calibrated parameter combination did not ensure an exact match with the draught force. Another reason could be the inaccurate modelling of the bulk density, as a 2900 kgm^{-3} particle density may have resulted in an excessively high bulk density for

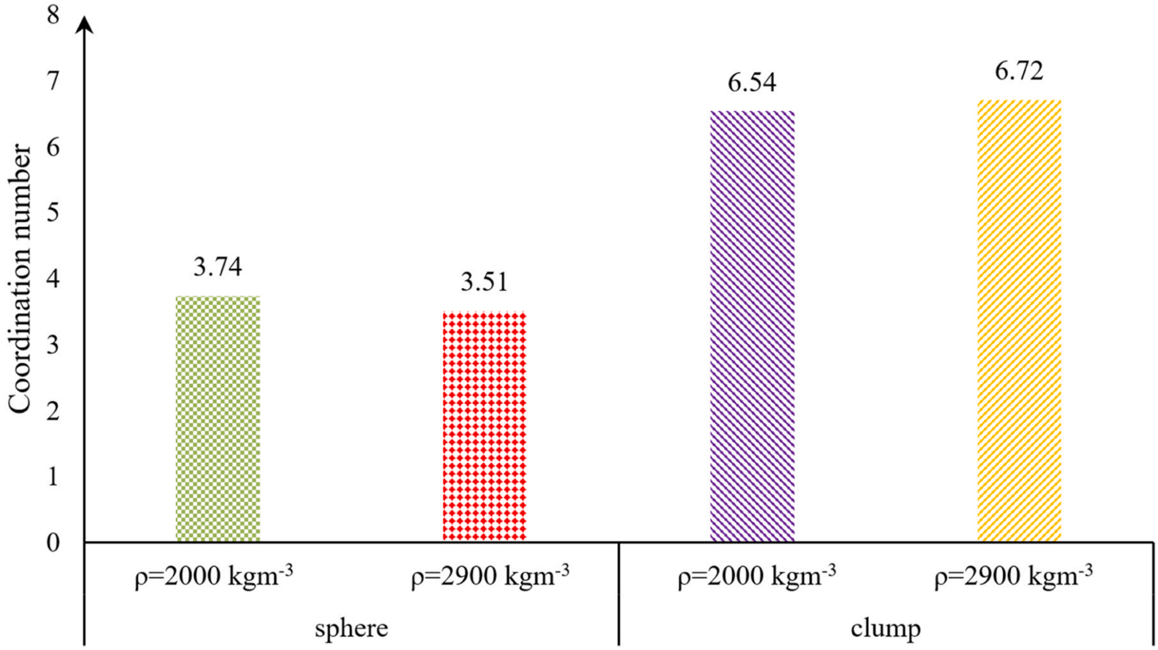

Fig. 11. Coordination number of the initial DEM particle assemblies.

the examined soil with 4.1 % dry based moisture content. Hence, in order to achieve a better agreement, the original soil particle density of 2900 kgm^{-3} was reduced. Although this reduced the difference between the measured and simulated draught force, it increased the difference between the measured and simulated horizontal CPR, so the reduction of the density was only possible to a limited extent. Therefore, our assumption is that, when using the same particle size and parameter combination to simulate geometries of different sizes, only a limited degree of agreement can be achieved between measurements and simulations. At a particle density of 2000 kgm^{-3} a compromise agreement was found in the simulations with the sweep tool and the horizontal CPR, so that, besides the soil particle solids density of 2900 kgm^{-3} the simulations were also run with a soil particle solids density of 2000 kgm^{-3}. Since a different gravitational deposition was performed for every particle shape and density combination to construct the particle assembly, each case resulted in a different bulk density. The spherical particles with a density of 2900 kgm^{-3} formed a particle assembly with 1402 kgm^{-3} bulk density, while the spherical particles with a density of 2000 kgm^{-3} formed a particle assembly with 1009 kgm^{-3} bulk density, the clump particles with a density of 2900 kgm^{-3} formed a particle assembly with 1129 kgm^{-3} bulk density and the clump particles with a density of 2000 kgm^{-3} formed a particle assembly with 785 kgm^{-3} bulk density. The applied material parameters can be found in Table 1. It can be seen that the mass of the soil particles was calculated based on the density value, and the mass of the displacement sensor was determined using a digital scale (Silvercrest® SKWS 5 A1, Hoyer Handel GmbH, Germany, 2–5000 g weighing range, 1 g accuracy). The parameters of the material pairs used for the spherical particles are given in Table 2., and the parameters of the material pairs used for clump particles are given in Table 3. In the simulations, the time step was set to 20 % of the Rayleigh time step (Tamás, 2018), which was $9.1827 \bullet 10^{-6}$ s for particles with a density of 2900 kgm^{-3}, and $7.6258 \bullet 10^{-6}$ s for particles with a density of 2000 kgm^{-3}. In this way a sufficiently stable and convergent outcome was ensured.

3. Results

3.1. Results of HP and displacement sensor measurements and simulations

The velocity field of the particle assembly with a spherical particle shape and 2900 kgm^{-3} density derived from the HP simulations is shown in Fig. 9. It is observable that the HP body holding the penetrometer cone pushes the particles forward, which gradually accumulate in front of the HP, and as a result, as the HP advances through the particle assembly the particles that are farther in front of it also start to move, i.e. the zone of moving particles in front of the HP expands. At a HP displacement of 2 m, the surface particles located more than half a meter in front of the HP were observed to start to move, whereas at the depth of the penetrometer cone, the particles started to move when they were 300 mm in front of the HP body (Fig. 9. c). Since the end of the cone is less than 300 mm in front of the HP body, the movement of the HP body in the simulation—and presumably also in the measurement—influenced the measured CPR value.

Fig. 10. shows the movement of the displacement sensor measured for the particle assembly with a spherical particle shape and a density of 2900 kgm^{-3}. In the figure, the soil particles and the HP have been made 90 % transparent, so that the displacement sensor can be seen, as otherwise it would be hidden behind the soil particles or the HP. It can be observed that the displacement sensor does not move during the first 1000 mm of displacement of the HP (Fig. 10. a), but then, when the HP approaches it, the displacement sensor moves forward and upward together with the particles that pile up in front of the HP (Fig. 10. b). At a HP displacement of 2000 mm, the displacement sensor is pushed to one side of the HP (Fig. 10. c) and then it is left behind by the HP, so that it falls back into the furrow created behind the HP. Its final position is 441.4 mm ahead, 18.7 mm higher, and 40.7 mm to the left (Fig. 10. d) of its original location. Furthermore, it is also observable that the yellow particles, which were initially above the displacement sensor, scattered behind the displacement sensor and fell back into the furrow made by the HP (Fig. 10. d).

The HP simulation that was performed on the assembly of clump elements with a density of 2900 kgm^{-3} produced the velocity field of the assembly shown in Fig. 12. It is observable that, compared to the

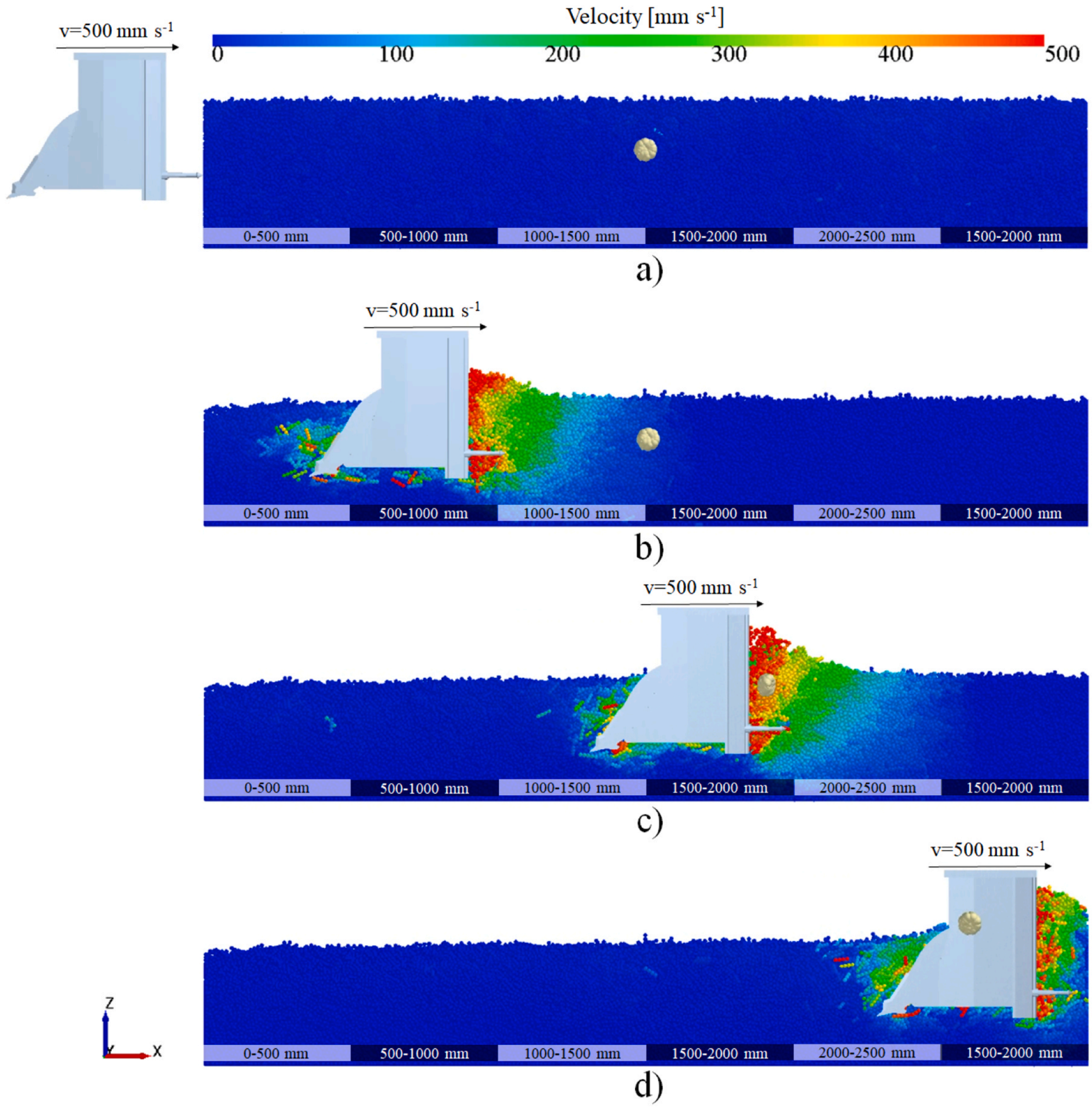

Fig. 12. Velocity of the assembly with clump particles with 2900 kgm^{-3} density at a) 0 mm, b) 1000 mm, c) 2000 mm and d) 3000 mm HP displacement (the velocity of the HP is indicated by vector **v**).

spherical particles, the clump particles accumulated even more in front of the penetrometer. This is because, due to their elongated shape, it is more likely for two elements to come into contact with each other and thus to prevent each other's movement, i.e. the average coordination number of the clump particles, which is defined as the average number of contacts between the particles, is significantly higher than that of the spherical particles (Fig. 11.). This leads to clumping and slower particle movement. At a HP displacement of 1 m, the particles started to move on the surface more than half a metre in front of the HP body (Fig. 12. b), while at the depth of the penetrometer cone, the particles were already set in motion when they were 350 mm in front of the HP body (Fig. 12. b and c). Since the end of the cone precedes the HP body supporting the cone by less than 350 mm, the movement of the particles influenced the measured soil resistance value in the simulation and presumably also in the measurement.

The movement of the displacement sensor in the assembly made up of clump particles with a density of 2900 kgm^{-3} is shown in Fig. 13. Similarly to in Fig. 10, the soil particles and the penetrometer have been made 90 % transparent in this figure too. Initially, during the first 1000 mm of displacement of the HP (Fig. 13. a), no movement was detected. However, as the HP approaches, the displacement sensor moves slightly forward and downward, accompanied by the accumulation of particles in front of the HP. Subsequently, it moves significantly forward and upward (Fig. 13. b). At a HP displacement of 2000 mm, the displacement sensor aligns with one side of the HP and moves along with it until the simulation concludes. This differs from the results obtained with spherical particles, because in that simulation the HP moved beyond the displacement sensor at the end of the simulation. Finally, the displacement sensor undergoes a slight downward movement, settling 1097 mm forward, 135 mm upward, and 66 mm to the right of its initial position (Fig. 13. d). Additionally, it is observable that the yellow particles, initially positioned above the displacement sensor, mostly disperse behind it, returning to the furrow created by the HP. Nonetheless, a few particles remained in front of the HP throughout the simulation (Fig. 13. d). In summary, the yellow particles covered a greater distance in the form of clump particles compared to spherical particles, a result which can also be attributed to the fact that clump particles locked the movement of each other more than spherical particles, thus remaining in front of the HP for more time and a longer distance.

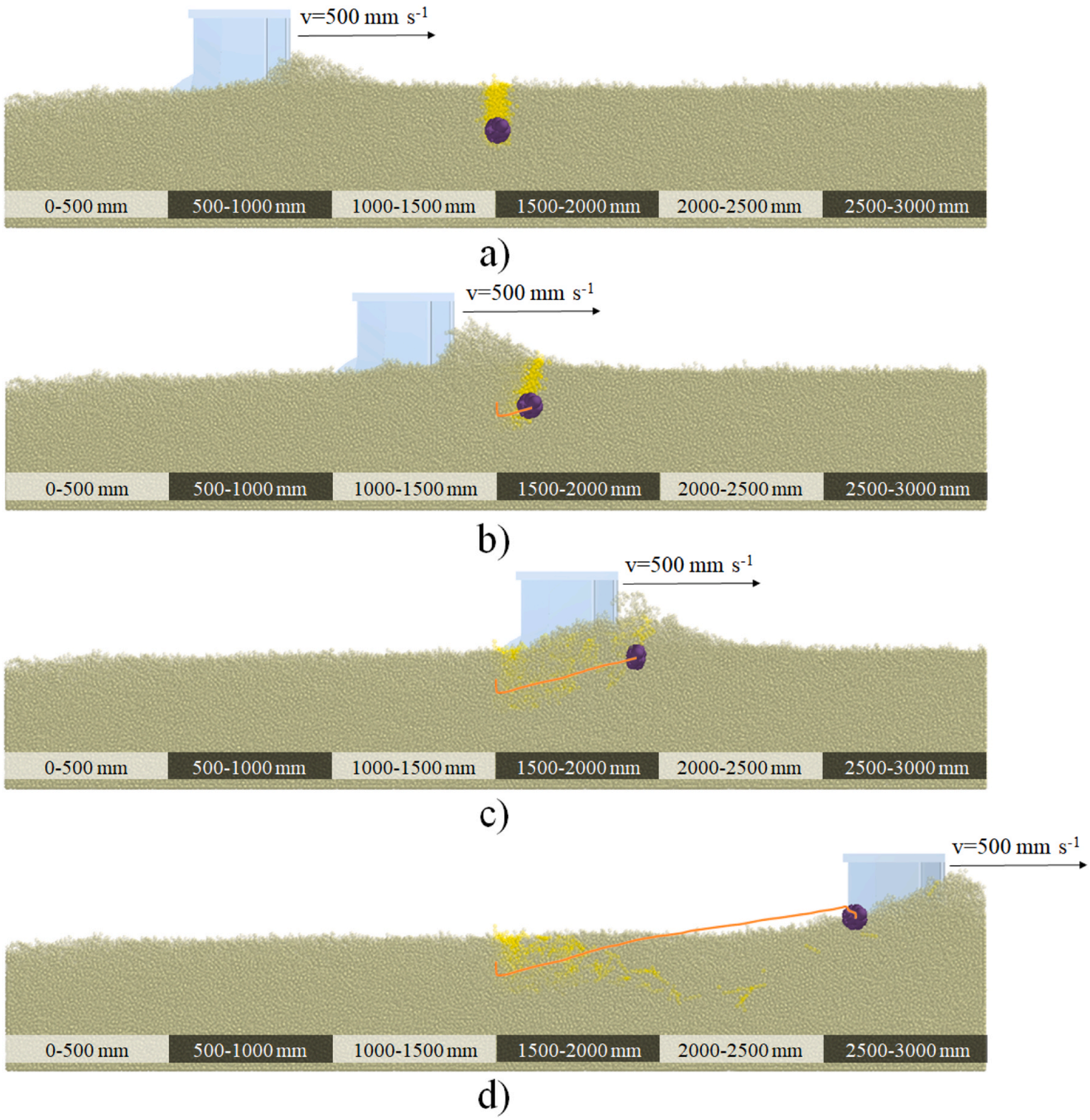

Fig. 13. Movement of the displacement sensor in the simulation of the HP measurement with clump particle shape and 2900 kgm^{-3} density at a) 1000 mm, b) 1500 mm, c) 2000 mm, d) 3000 mm HP displacements (due to the visibility of the displacement sensor, the soil particles and the HP were made 90 % transparent, the velocity of the HP is indicated by vector **v**, the trajectory path of the displacement sensor is indicated by an orange line, and the particles which were initially above the displacement sensor are coloured yellow).

Fig. 14. shows the change of the horizontal CPR during the simulations as a function of the displacement of the HP, as well as the horizontal CPR measured in the middle 3 m of the measuring section. It can be seen that, in the case of 2900 kgm^{-3} particle density, after the initial increase, the simulated CPR values started to fluctuate around the average of the measured CPR value with a good approximation, even for spherical and clump particles, while in the simulation with a 2000 kgm^{-3} particle density the simulated average horizontal CPR values remained below the measured average value. In the last 1 m of the CPR's progress, the simulated CPR values started to increase in all the investigated configurations, due to the wall effect. The relative differences between the measured and simulated average horizontal CPR values are 7.2 % for spherical particles with a density of 2900 kgm^{-3}, 26.2 % for clump particles with a density of 2900 kgm^{-3}, 21.2 % for spherical particles with a density of 2000 kgm^{-3} and 18.1 % for clump particles with a density of 2000 kgm^{-3}. Fig. 14 d) shows the resulting simulated horizontal CPR values for spherical particles where the HP body was removed and only the cone was moved in the particle assembly. It can be seen that the horizontal CPR values are slightly lower when the penetrometer body is removed and only the cone is moved through the particle assembly. This can be explained by the fact that the penetrometer body compacted the soil in front of it, resulting in higher horizontal CPR values than the original CPR of the undisturbed soil. It can thus be surmised that, in order to measure the horizontal CPR more accurately, the rod length of the HP cone needs to be extended in the future. Nevertheless, the simulated and measured horizontal CPR values remained comparable as the soil compaction effect of the penetrometer body was present in both the simulations and the measurements.

Fig. 15. shows the trajectory paths of the displacement sensor in the HP measurement and in the simulations. It can be seen that the projections of the measured and simulated trajectory paths in the x-z plane have similar characteristics. In all cases, the displacement sensor initially moved downwards, then upwards, and finally downwards again (Fig. 15. a). The trajectory projections of the measured and simulated

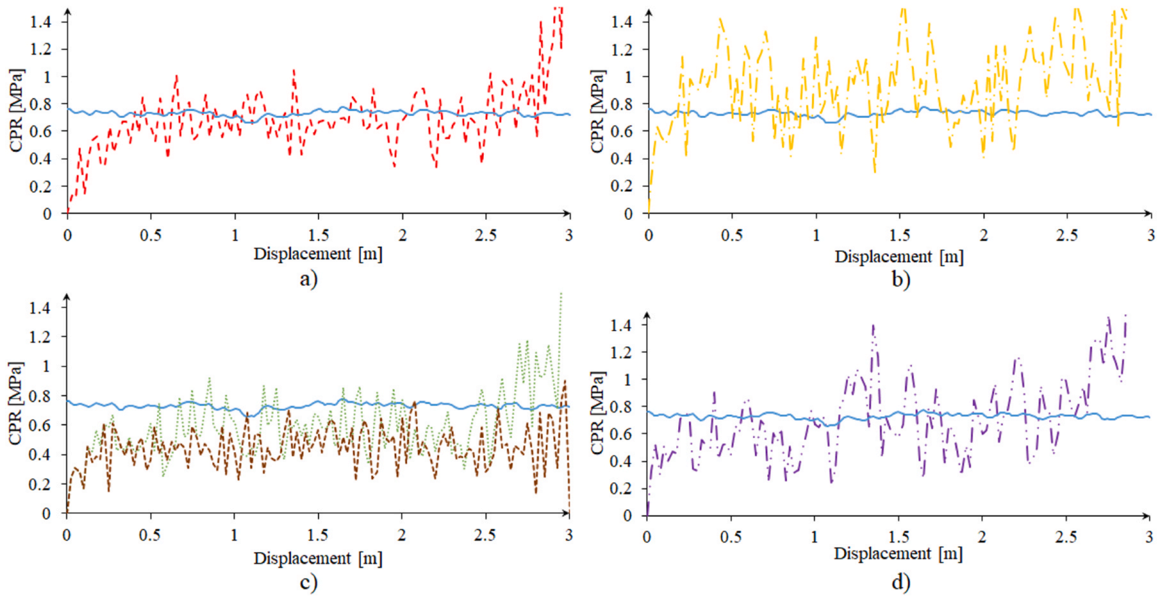

Fig. 14. Horizontal CPR in the function of HP displacement in the case of — measurements and simulations of a) -- spherical particles with 2900 kgm^{-3} density, b) -·- clump particles with 2900 kgm^{-3} density, c) ··· spherical particles with 2000 kgm^{-3} density, - - spherical particles with 2000 kgm^{-3} density with the HP body removed and only the cone present and d) -··- clump particles with 2000 kgm^{-3} density.

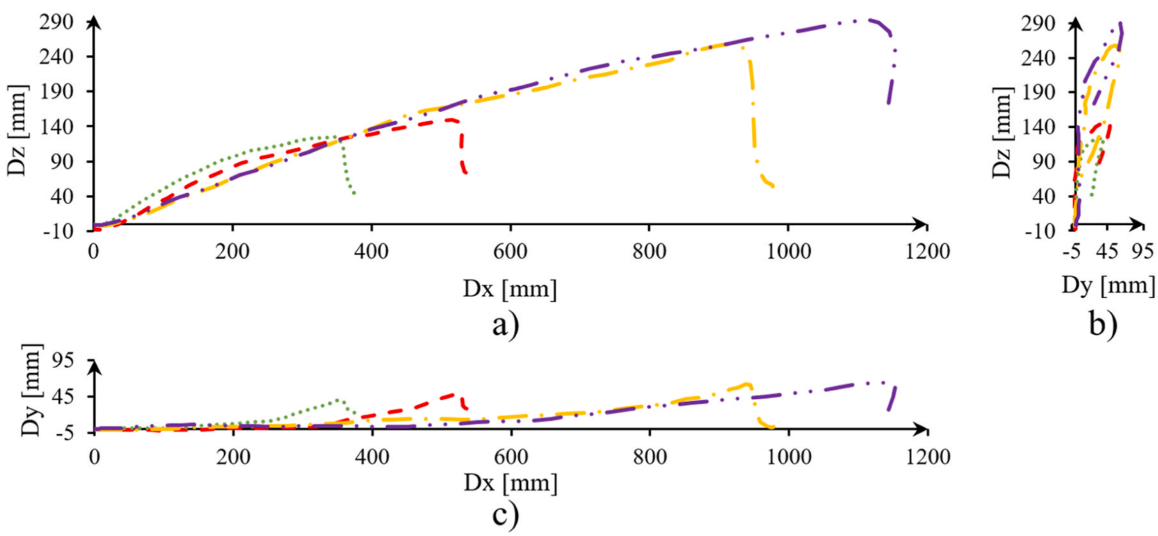

Fig. 15. Trajectory path of the displacement sensor in the case of HP — measurement and simulations of -- spherical particles with 2900 kgm^{-3} density, -·- clump particles with 2900 kgm^{-3} density, ··· spherical particles with 2000 kgm^{-3} density and -··- clump particles with 2000 kgm^{-3} density, projection of the trajectories to the a) x-z plane, b) y-z plane and c) x-y plane.

data in the other two planes show a smaller degree of agreement (Fig. 15. b and c). It can also be observed that when simulations were run with spherical particles, the simulated trajectory matched the actual measured trajectory better than of the trajectories in simulations run with clump particles. When the simulations used clump particles, the displacement sensor travelled a significantly longer distance in the longitudinal and vertical direction than the measured values, which can be explained by the fact that elongated clump elements obstructed the movement of the displacement sensor more, so the clump particles and the displacement sensor collectively remained in front of the HP for a longer distance. The average deviation of the simulated trajectory path of the displacement sensor from the measured trajectory path was 5.2 % in the case of spherical particles with a density of 2900 kgm^{-3}, 34.3 % in the case of clump particles with a density of 2900 kgm^{-3}, 7.6 % in the case of spherical particles with a density of 2000 kgm^{-3} and 29.9 % in the case of clump particles with a density of 2000 kgm^{-3}. The deviations observed could be attributed to the fact that real soil particles are smaller than the particles in the simulations, which may have caused a difference in the contact behaviour and relative movement between the soil particles and the displacement sensor. It may therefore be possible to further increase the degree of agreement by reducing the simulated particle size, the errors in the measured data and by more precisely calibrating the parameters in the simulation.

3.2. *Results of sweep tool measurement and simulations*

The draught force of the sweep tool in the function of tool displacement is shown in Fig. 16. It is observable that in the simulations, after the initial increase, the draught force fluctuates around a particular value, which always exceeds the measured value, and at the end of the

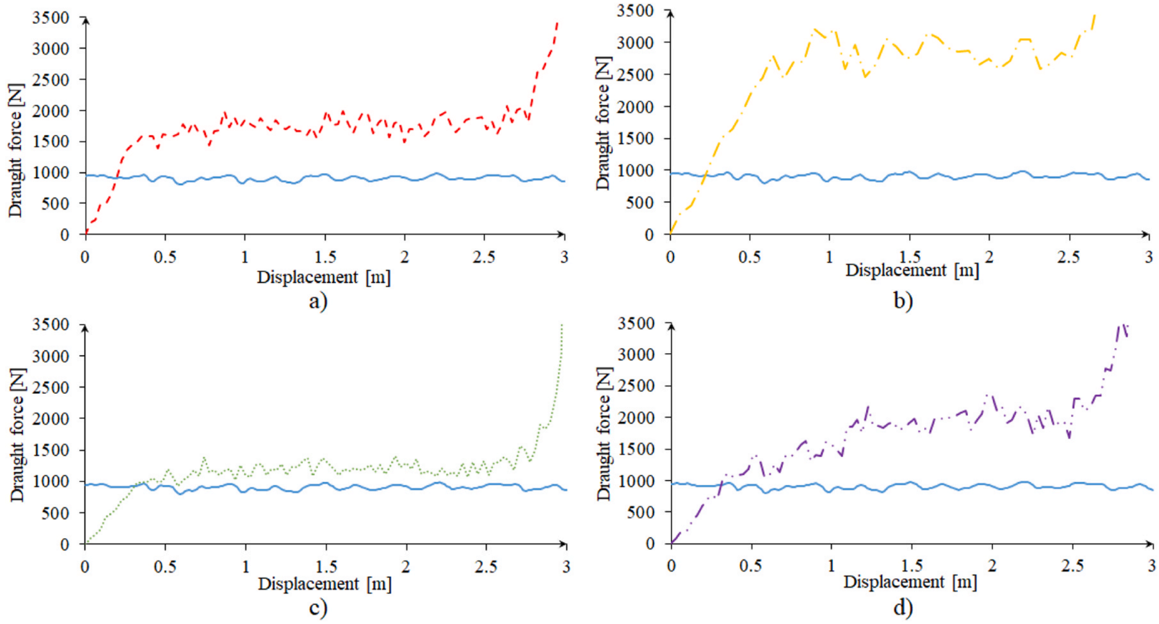

Fig. 16. Draught force acting on the sweep tool in the function of tool displacement in the case of — measurement and simulations of a) -- spherical particles with 2900 kgm^{-3} density, b) -·- clump particles with 2900 kgm^{-3} density, c) ··· spherical particles with 2000 kgm^{-3} density and d) -··- clump particles with 2000 kgm^{-3} density.

simulations the draught force increases due to the wall effect. A better match with the measurement was achieved for the spherical particles than for the clump particles, where the draught force significantly exceeded the measured value. Reducing the density of particles resulted in the simulated draught force values being closer to the measured values. The relative difference between the average values of the measured and simulated draught force was 94.6 % for spherical particles with a density of 2900 kgm^{-3}, 210.9 % for clump particles with a density of 2900 kgm^{-3}, 31.8 % for spherical particles with a density of 2000 kgm^{-3} and 99.8 % for clump particles with a density of 2000 kgm^{-3}.

Fig. 17. shows the velocity field of the particle assemblies derived from the simulations of the soil-sweep interaction at a tool displacement of 1.5 m. It can be seen that in all the simulations, the particles piled up in front of the sweep tool by moving forward and upwards, then, passing behind the sweep tool, the particles move downwards, falling back into the furrow formed by the tool. It can also be observed that the clump particles (Fig. 17. a and b) pile up to a greater extent in front of the tool, resulting in a greater draught force than that resulting from the spherical particles (Fig. 17. c and d), and that the particles with a higher particle density and bulk density also piled up to a greater extent in front of the tool (Fig. 17. b and d) and therefore resulted in a higher draught force compared to particles with a lower particle density and bulk density (Fig. 17. a and c). On the other hand, due to greater inertia, particles with a higher density moved at a lower speed than particles with a lower density.

The trajectory paths of the displacement sensor in the soil-sweep interaction simulations are shown in Fig. 18. It is observable that larger displacements occurred when clump particles were simulated, which, similarly to the simulations of the HP measurement, can be explained by more frequent particle contacts due to the elongated shape of the particles.

3.3. Results of the vertical penetrometer measurement and simulations

The measured and simulated vertical CPR values are shown in Fig. 19. as a function of soil depth. It can be seen that the simulations overestimated the CPR compared to the measurements up to a depth of 20–30 cm, and underestimate it at deeper levels. However, even considering this discrepancy, there is a good agreement between the simulations and the measurement, because the simulated values are always within the standard deviation of the measured values. The correlation error between the average values of the measured and simulated CPR was 7.7 % for spherical particles with a density of 2900 kgm^{-3}, 13.2 % for clump particles with a density of 2900 kgm^{-3}, 8.7 % for spherical particles with a density of 2000 kgm^{-3} and 55.2 % for clump particles with a density of 2000 kgm^{-3}. The higher correlation error of the clump particles can be explained by a similar phenomenon as occurred in the other simulations: The clump particles locked the movement of each other and the penetrometer, thus the measured CPR was overestimated. Moreover, similarly to the horizontal CPR, the reduction in density also reduced the vertical CPR, which resulted in a slight underestimation of the vertical CPR and an increase in the correlation error in the case of spherical particles with 2000 kgm^{-3} density.

4. Discussion

The average deviations of the results of the simulations from the empirically measured results are shown in Table 4. It can be seen that when spherical particles were simulated, the results of the simulations are closer to the measurement results than when clumps of particles were modelled. Simulating clump particles in soil modelling was therefore found not to be a suitable approach when using the hysteretic spring contact model. When spherical particles were modelled, the particles with a density of 2900 kgm^{-3} closely approximated the measured average horizontal CPR (7.2 % error) and the trajectory path of the displacement measuring sensor (5.2 % relative error), but overestimated the average value of the draught force acting on the sweep tool (94.6 % relative error). On the other hand, when the spherical particles were simulated at a density of 2000 kgm^{-3}, there was a greater deviation from the measured average horizontal CPR (21.2 % relative error) and the trajectory of the displacement sensor (7.6 % error), but the average measured and simulated draught force acting on the sweep tool showed significantly more agreement (31.8 % relative error). Therefore, it may be assumed that, to take size variations into consideration, the soil particles need to be modelled with different sized

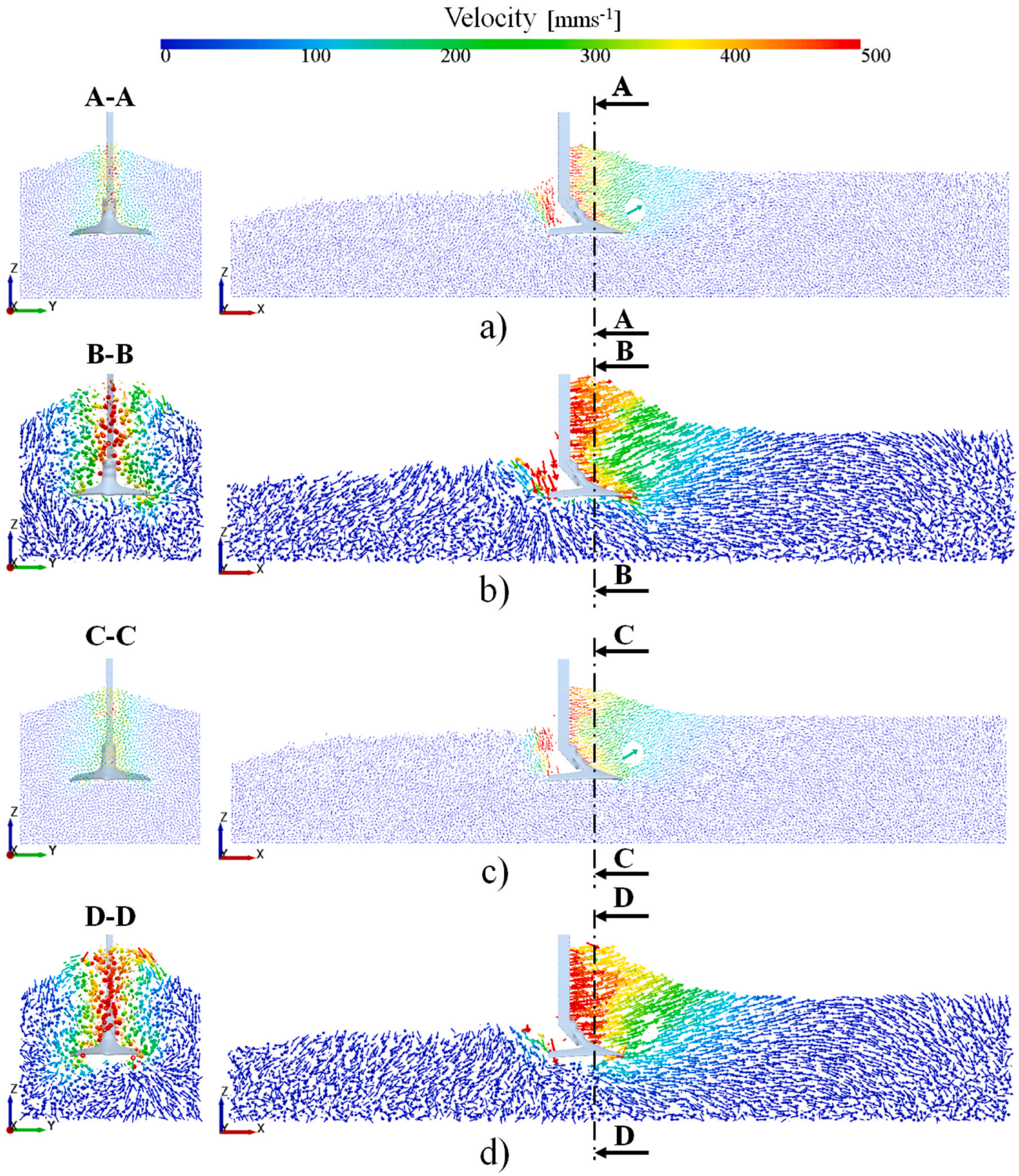

Fig. 17. Velocity field of particles in the soil sweep tool simulations at 1.5 m tool displacement in the case of a) spherical particles with 2900 kgm^{-3} density, b) clump particles with 2900 kgm^{-3} density, c) spherical particles with 2000 kgm^{-3} density, and d) clump particles with 2000 kgm^{-3} density.

particles and with different discrete element parameter combinations, in order to accurately model the contact of bodies of significantly different sizes with the soil. Using the same particle size and parameter combination, only a limited degree of agreement can be achieved between measurements and simulations. The average error value, taking into account the four measurements and simulations together, was the smallest (23.1 % relative error) when the model comprised an assembly made up of spherical particles with a particle density of 2000 kgm^{-3}, i.e., taking into account all the examined aspects, this assembly modelled the tested sandy soil most accurately.

5. Conclusion

The main novelty of the study is that during the DEM parameter calibration of a sample of sandy soil, the results of four different measurement procedures were taken into account at the same time, thereby creating a DEM model that describes the examined soil well from several points of view. The measurements and simulations were made using an in-house developed HP, a displacement measuring sensor placed in the soil, a sweep tool and a vertical penetrometer in a sample of sandy soil with a dry based moisture content of 4.1 %, with the measurements conducted in a laboratory soil bin facility. The simulations were performed with Altair EDEM® software using spherical and clump elements. Based on the results, the following conclusions can be drawn.

The developed HP and the displacement sensor placed in the soil can provide sufficiently accurate information about the soil CPR and the internal displacements of the soil for DEM parameter calibration.

During the parameter calibration, it was found that for the hysteretic

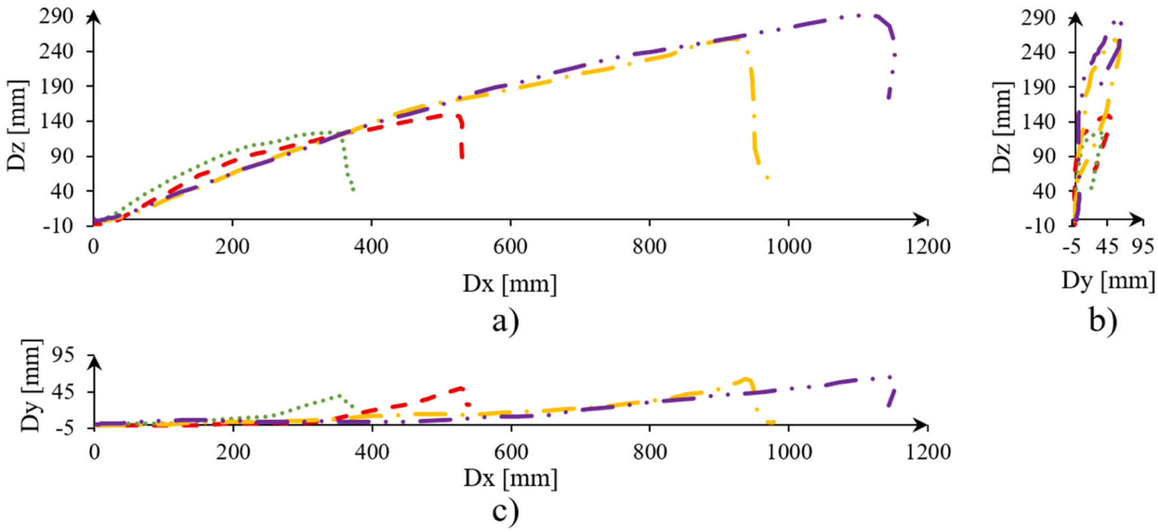

Fig. 18. Trajectory paths of the displacement sensor in the case of soil sweep interaction simulations of -- spherical particles with 2900 kgm^{-3} density, -·- clump particles with 2900 kgm^{-3} density, ··· spherical particles with 2000 kgm^{-3} density and -··- clump particles with 2000 kgm^{-3} density, projection of the trajectories to the a) x-z plane, b) y-z plane and c) x-y plane.

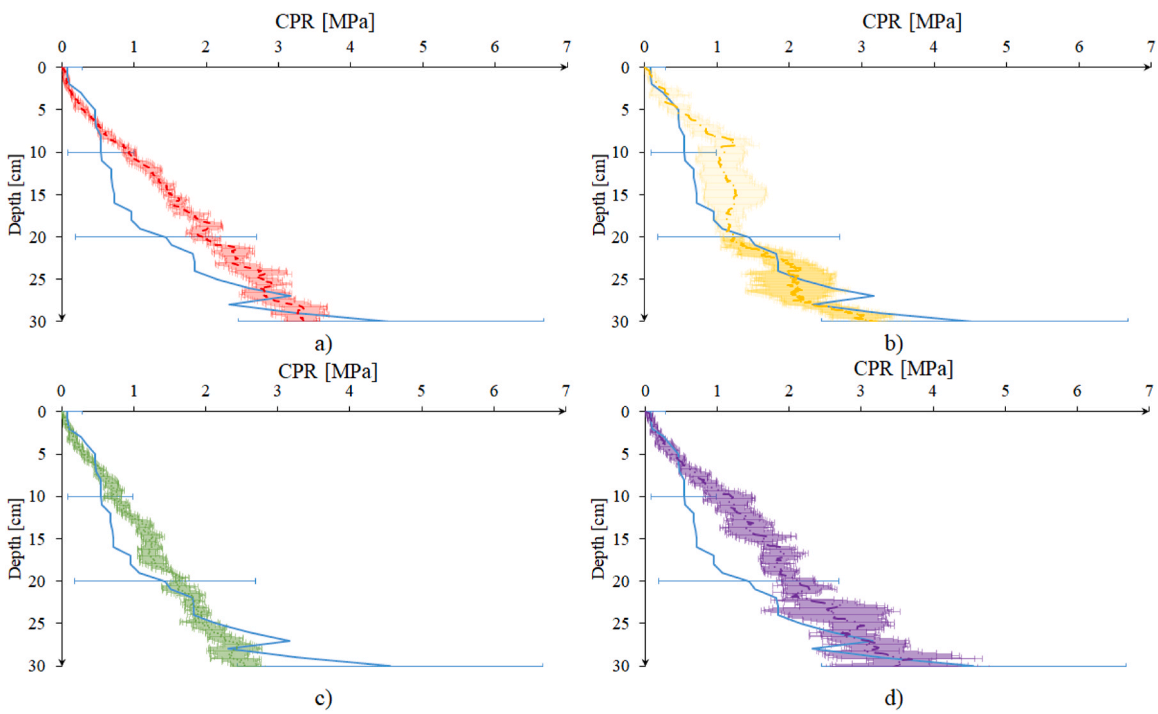

Fig. 19. Vertical CPR in the function of soil depth in the case of – measurements and simulations of a) – spherical particles with 2900 kgm^{-3} density, b) -·- clump particles with 2900 kgm^{-3} density, c) ··· spherical particles with 2000 kgm^{-3} density and d) -·- clump particles with 2000 kgm^{-3} density.

spring contact model, particle size and geometry which were applied, a closer match between the measurements and simulations was achieved by using spherical elements, because clump elements, due to their elongated shape, stuck together and excessively piled up in front of the tools and measuring devices, which resulted in higher than measured horizontal CPR, sweep tool draught force and longer longitudinal and vertical displacements of the displacement sensor.

The DEM model that had been calibrated by adjusting the friction parameters in line with the measured and simulated horizontal CPR results overestimated the draught force in the sweep tool simulations, which can be explained by the assumption that when using the same particle size and parameter combination to simulate geometries of different sizes, only a limited degree of agreement can be achieved between measurements and simulations. By reducing the particle's density it was possible to achieve a compromise match with the measured horizontal CPR and the sweep tool draught force data.

Studying the sweep tool simulations revealed that particles with a higher density pile up in front of the tool to a greater extent, thus resulting in a greater draught force, but at the same time, due to the greater inertia, particles of a higher density move at a lower speed.

The results of the vertical penetrometer simulations were within the standard deviation of the measurement results for all depths, thus effectively validating the parameter combination calibrated with spherical elements. It can therefore be concluded that the soil model

Table 4
Average deviations of the simulated results from the measured results.

	sphere		clump	
	ρ = 2900 kgm^{-3}	ρ = 2000 kgm^{-3}	ρ = 2900 kgm^{-3}	ρ = 2000 kgm^{-3}
horizontal CPR relative error [%]	7.2	21.2	26.2	18.1
sweep tool draught force relative error [%]	94.6	31.8	210.9	99.8
vertical CPR correlation error [%]	7.7	8,7	13.2	55.2
displacement sensor trajectory mean deviation [%]	5.2	7.6	34.3	29.9
max deviation [%]	94.6	31.8	210.9	99.8
average deviation [%]	41.9	23.1	99.1	60.6

created with spherical elements more accurately simulates the compactness of the tested soil, the internal movement of the soil and the draught force of tillage tools, which suggests that DEM parameter combinations of the real cultivated areas could be calibrated by applying the proposed combined calibration method using horizontal penetrometer, vertical penetrometer, soil displacement sensor and possibly sweep tool measurements. The tillage parameters could then be optimised by running DEM simulations which are more cost and time effective than taking field measurements. Applying the resulting optimal parameters in practice would then presumably reduce the cost and increase the effectiveness of real tillage processes. For example, in drought-prone regions the soil moisture content retention of a field could be ensured at a lower cost and in a shorter time.

Nevertheless, in order to more accurately match the results of the simulations and measurements, the authors recommend the use of calibration procedures supported by stochastic local search techniques, for example genetic algorithms. Furthermore, since the test was only carried out in wet sandy soil, in order to create a more generally applicable soil model, different speeds, different soil types, different tool geometries, measurement procedures and additional DEM contact models could be used to model the soil, and the effect of soil moisture could also be the focus of future studies.

CRediT authorship contribution statement

Bence Szabó: Methodology, Data curation, Conceptualization. **László Pásthy:** Writing – original draft, Visualization, Validation, Software, Project administration, Investigation. **Kornél Tamás:** Writing – review & editing, Supervision, Resources, Project administration, Methodology, Investigation, Funding acquisition, Data curation, Conceptualization.

Declaration of Competing Interest

The authors declare that they have no known competing financial interests or personal relationships that could have appeared to influence the work reported in this paper.

Data availability

Data will be made available on request.

Acknowledgements

The authors gratefully acknowledge the assistance of the staff at the Institute of Technology of the Hungarian University of Agriculture and Life Sciences for allowing the use of their testing facilities and for providing practical support while the measurements were being carried out. Special thanks are due to László Kovács and Árpád Wágner for their help in IMU sensor development, to Zoltán Hudoba for his support during the experiments and to József Balázs Gräff and Balázs Janzsó for their help with proof reading. This paper was supported by the János Bolyai Research Scholarship of the Hungarian Academy of Sciences. The research reported in this paper is part of project no. TKP-6-6/PALY-2021, implemented with the support of the Ministry of Innovation and Technology of Hungary under the aegis of the National Research, Development and Innovation Fund, financed under the TKP2021-NVA funding scheme. The project was supported by the Doctoral Excellence Fellowship Programme (DCEP), which is funded by the National Research Development and Innovation Fund of the Ministry of Culture and Innovation and the Budapest University of Technology and Economics, under a grant agreement with the National Research, Development and Innovation Office. This research was also supported by the ÚNKP, funded by the National Research Development and Innovation Fund under grant number ÚNKP-23–5-BME-80. This paper was supported by the Hungarian Scientific Research Fund (NKFIH FK-146067).

References

Acharya, C.L., Kapur, O.C., Dixit, S.P., 1998. Moisture conservation for rainfed wheat production with alternative mulches and conservation tillage in the hills of north-west India. Soil Tillage Res. 46, 153–163.

Alihamsyah, T., Humphries, E.G., Bowers, Jr, C.G., 1990. A technique for horizontal measurement of soil mechanical impedance. Trans. ASAE 33, 0073–0077. https://doi.org/10.13031/2013.31296.

ASABE Standards, 2006b. American Society of Agricultural and Biological Engineers ASABE Standard S313.3 FEB04. Soil Cone Penetrometer, St. Joseph, ML., USA.

ASABE Standards, 2006a. American society of agricultural and biological engineers ASABE standard ASAE EP542 FEB99. St. Joseph, ML., USA: Procedures for Using and Reporting Data Obtained with the Soil Cone Penetrometer.

Bahrami, M., Naderi-Boldaji, M., Ghanbarian, D., Ucgul, M., Keller, T., 2020. Simulation of plate sinkage in soil using discrete element modelling: Calibration of model parameters and experimental validation. Soil Tillage Res. 203, 104700.

Bekele, B., Habtemariam, T., Gemi, Y., 2022. Evaluation of conservation tillage methods for soil moisture conservation and maize grain yield in low moisture areas of SNNPR, Ethiopia. Water Conserv. Sci. Eng. 7, 119–130. https://doi.org/10.1007/s41101-022-00129-0.

Bruno, C.H., Tripodi, E., Werner, D., Windows-Yule, C., Spyropoulos, F., 2024. The performance of rotating membrane emulsification in the presence of baffles: Insights from flux experiments, microstructural analysis, and positron emission particle tracking. Chem. Eng. Sci. 284, 119476.

Chen, Y., Cavers, C., Tessier, S., Monero, F., Lobb, D., 2005. Short-term tillage effects on soil cone index and plant development in a poorly drained, heavy clay soil. Soil Tillage Res. 82, 161–171. https://doi.org/10.1016/j.still.2004.06.006.

Cheng, H., Shuku, T., Thoeni, K., Tempone, P., Luding, S., Magnanimo, V., 2018. Grain Learning: Bayesian Calibration of DEM Models and Validation Against Elastic Wave Propagation. In: Wu, W., Yu, H.-S. (Eds.), Proceedings of China-Europe Conference on Geotechnical Engineering, Springer Series in Geomechanics and Geoengineering. Springer International Publishing, Cham, pp. 132–135. https://doi.org/10.1007/978-3-319-97112-4_29.

Do, H.Q., Aragón, A.M., Schott, D.L., 2017. Automated discrete element method calibration using genetic and optimization algorithms. : EPJ Web Conf. EDP Sci. 15011.

Grabowski, A., Nitka, M., Tejchman, J., 2021. Comparative 3D DEM simulations of sand–structure interfaces with similarly shaped clumps versus spheres with contact moments. Acta Geotech. 16, 3533–3554. https://doi.org/10.1007/s11440-021-01255-0.

Gürsoy, S., Chen, Y., Li, B., 2017. Measurement and modelling of soil displacement from sweeps with different cutting widths. Biosyst. Eng. 161, 1–13. https://doi.org/10.1016/j.biosystemseng.2017.06.005.

Hall, H.E., Raper, R.L., 2005. DEVELOPMENT AND CONCEPT EVALUATION OF AN ON-THE-GO SOIL STRENGTH MEASUREMENT SYSTEM [WWW Document]. URL. https://doi.org/10.13031/2013.18311 (accessed 10.5.23).

Hemmat, A., Khorsandy, A., Masoumi, A.A., Adamchuk, V.I., 2009. Influence of failure mode induced by a horizontally operated single-tip penetrometer on measured soil resistance. Soil Tillage Res. 105, 49–54. https://doi.org/10.1016/j.still.2009.05.003.

Katagiri, J., 2019. A novel way to determine number of spheres in clump-type particle-shape approximation in discrete-element modelling. Géotechnique 69, 620–626. https://doi.org/10.1680/jgeot.18.P.021.

Kim, K., Prezzi, M., Salgado, R., Lee, W., 2008. Effect of Penetration Rate on Cone Penetration Resistance in Saturated Clayey Soils. J. Geotech. Geoenviron. Eng. 134, 1142–1153. https://doi.org/10.1061/(ASCE)1090-0241(2008)134:8(1142).

Kotrocz, K., Mouazen, A.M., Kerényi, G., 2016. Numerical simulation of soil–cone penetrometer interaction using discrete element method. Comput. Electron. Agric. 125, 63–73. https://doi.org/10.1016/j.compag.2016.04.023.

Marigo, M., Davies, M., Leadbeater, T., Cairns, D.L., Ingram, A., Stitt, E.H., 2013. Application of Positron Emission Particle Tracking (PEPT) to validate a Discrete Element Method (DEM) model of granular flow and mixing in the Turbula mixer. Int. J. Pharm. 446, 46–58.

Milkevych, V., Munkholm, L.J., Chen, Y., Nyord, T., 2018. Modelling approach for soil displacement in tillage using discrete element method. Soil Tillage Res. 183, 60–71. https://doi.org/10.1016/j.still.2018.05.017.

Mouazen, A.M., Dumont, K., Maertens, K., Ramon, H., 2003. Two-dimensional prediction of spatial variation in topsoil compaction of a sandy loam field-based on measured horizontal force of compaction sensor, cutting depth and moisture content. Soil Tillage Res. 74, 91–102. https://doi.org/10.1016/S0167-1987(03)00123-5.

Naderi-Boldaji, M., Alimardani, R., Hemmat, A., Sharifi, A., Keyhani, A., Tekeste, M.Z., Keller, T., 2014. 3D finite element simulation of a single-tip horizontal penetrometer–soil interaction. Part II: Soil bin verification of the model in a clay-loam soil. Soil Tillage Res. 144, 211–219. https://doi.org/10.1016/j.still.2014.03.008.

Naderi-Boldaji, M., Sharifi, A., Alimardani, R., Hemmat, A., Keyhani, A., Loonstra, E.H., Weisskopf, P., Stettler, M., Keller, T., 2013. Use of a triple-sensor fusion system for on-the-go measurement of soil compaction. Soil Tillage Res. 128, 44–53.

Nisha, K., Upadhyay, G., Patel, B., Choudhary, S., Rani, V., 2023. A tractor hydraulic assisted embedded microprocessor-based penetrometer for soil compaction measurement. J. Terra 110, 1–12.

Pásthy, L., Farkas, Z.J., Haba, T., Tamás, K., 2024. Development of a multi-way coupled discrete-finite element method simulation procedure for modelling soil-passive vibration tool interaction. Comput. Electron. Agric. 216, 108459.

Pires-Sturm, A.P., DeJong, J.T., 2023. Cone Penetration Resistance in Coarse-Grained Gravelly Soils. J. Geotech. Geoenviron. Eng. 149, 04022120 https://doi.org/10.1061/(ASCE)GT.1943-5606.0002934.

Roessler, T., Richter, C., Katterfeld, A., Will, F., 2019. Development of a standard calibration procedure for the DEM parameters of cohesionless bulk materials–part I: Solving the problem of ambiguous parameter combinations. Powder Technology 343, 803–812.

Tamás, K., 2018. The role of bond and damping in the discrete element model of soil-sweep interaction. Biosyst. Eng. 169, 57–70.

Tamás, K., Bernon, L., 2021. Role of particle shape and plant roots in the discrete element model of soil–sweep interaction. Biosyst. Eng. 211, 77–96. https://doi.org/10.1016/j.biosystemseng.2021.09.001.

Tamás, K., Jóri, I.J., Mouazen, A.M., 2013. Modelling soil–sweep interaction with discrete element method. Soil Tillage Res. 134, 223–231.

Topakci, M., Unal, I., Canakci, M., Celik, H.K., Karayel, D., 2010. Design of a horizontal penetrometer for measuring on-the-go soil resistance. Sensors 10, 9337–9348. https://doi.org/10.3390/s101009337.

Ucgul, M., Fielke, J.M., Saunders, C., 2014. Three-dimensional discrete element modelling of tillage: determination of a suitable contact model and parameters for a cohesionless soil. Biosyst. Eng. 121, 105–117. https://doi.org/10.1016/j.biosystemseng.2014.02.005.

Ucgul, M., Fielke, J.M., Saunders, C., 2015. Defining the effect of sweep tillage tool cutting edge geometry on tillage forces using 3D discrete element modelling. Inf. Process. Agric. 2, 130–141.

Ucgul, M., Saunders, C., Fielke, J.M., 2018. Comparison of the discrete element and finite element methods to model the interaction of soil and tool cutting edge. Biosyst. Eng. 169, 199–208. https://doi.org/10.1016/j.biosystemseng.2018.03.003.

Ucgul, M., Saunders, C., Fielke and, J.M., 2017. Discrete element modelling of tillage forces and soil movement of a one-third scale mouldboard plough. Biosyst. Eng. 155, 44–54.

Wágner, Á., Szabó, B., Kovács, L., Tamás, K., Grad-Gyenge, L., 2023. The development of a soil-movement measurement system to create more precise numeric soil models. In: 1st Workshop on Intelligent Infocommunication Networks, Systems and Services (WI2NS2). Budapest University of Technology and Economics, pp. 83–88.

Yang, S., Huang, D., 2023. Investigating the influence of inherent soil fabrics on reliquefaction resistance of sands using DEM-clump simulation. Comput. Geotech. 164, 105817.

Zeng, Z., Ma, X., Chen, Y., Qi, L., 2020. Modelling residue incorporation of selected chisel ploughing tools using the discrete element method (DEM). Soil Tillage Res. 197, 104505 https://doi.org/10.1016/j.still.2019.104505.